AN ABSTRACT OF THE THESIS OF

David R. Rector for the degree of Master of Science in Mechanical Engineering presented on May 6, 1985

Title: Implementation and Evaluation of a Participating Media Radiation Model in the TEMPEST Thermal-Hydraulic Computer Code

Abstract approved: Redacted for Privacy

Dennis K. Kreid

In this work, a method for solving the differential form of the radiative transfer equation was implemented into an existing three-dimensional thermal-hydraulic computer program known as TEMPEST. The method used was the P-1 approximation, where the angular distribution of the radiation intensity is represented by a truncated series of spherical harmonics.

To determine the accuracy and limits of P-1 formulation, a series of comparisons were made between TEMPEST results and existing solutions. Evaluations were made for problems involving thermal radiation only, radiation and conduction, and finally, radiation, conduction, and convection.

In general, the P-1 method yielded acceptable results for radiation problems with large optical thicknesses ($\tau_0 > 1.0$) or combined radiation and conduction problems with participating media. The accuracy of results for radiation problems involving little or no optical thickness are highly dependent on the geometry of the problem.

IMPLEMENTATION AND EVALUATION OF A PARTICIPATING MEDIA RADIATION MODEL IN THE TEMPEST THERMAL-HYDRAULIC COMPUTER CODE

by

David R. Rector

A Thesis

submitted to

Oregon State University

in partial fullfillment of
the requirements for the
degree of

Master of Science

Completed May 6, 1985

Commencement June 1985

APPROVED:

Redacted for Privacy

Professor of Mechanical Engineering in charge of major

Redacted for Privacy

Head of Department of Mechanical Engineering

Redacted for Privacy

Dean of Graduate School

Date thesis is presented May 6, 1985

Typed by Cathy Darby for David R. Rector

ACKNOWLEDGEMENT

I wish to express my sincere gratitude to my advisor, Dr. Dennis Kreid, for his guidance and encouragement during the preparation of my thesis. I would also like to thank the other members of my committee, Dr. William Kinsel, Dr. Richard Collingham, and Dr. Charles E. Smith, for their helpful suggestions.

Special thanks goes to those who gave me valuable technical assistance during my thesis, including Dr. Don Trent, who assisted me in working with the TEMPEST computer code, and Dr. Richard A. McCann, for his help in developing the numerical techniques for the radiation solution. Appreciation is also expressed to Battelle, Pacific Northwest Laboratory for its financial support.

I am deeply indebted to Cathy Darby for putting this thesis in its present form.

Finally, I thank my wife, Becky, and my children, Brian and Lydia, for the their patient love and support throughout this research.

TABLE OF CONTENTS

LIST OF FIGURES

LIST OF TABLES

NOMENCLATURE

a	absorption coefficient
a_p	Planck mean absorption coefficient (Eq. 4.3)
A	area
A_n^m	spatial coefficients in the spherical harmonic angular distribution of intensity
B	nondimensional emissive power (Eq. 4.10)
C	speed of propagation of light
C_p	specific heat
D	diameter
e_b	blackbody emissive power
I	radiation intensity
I_b	blackbody intensity
I_o	zeroth moment of intensity (Eq. 2.19)
I_i	first moment of intensity (Eq. 2.20)
I_{ij}	second moment of intensity (Eq. 2.21)
k	thermal conductivity
k_T	turbulent (eddy) thermal conductivity
$\hat{\ell}i$	direction cosine (Fig. 2.2)
L	participating media thickness
N	Stark number (Eq. 5.1)
P_n^m	associated Legendre polynomials
q	heat flux
Q	heat transfer rate
Q_R	nondimensional radiation heat transfer rate (Eq. 4.5)
Q_T	nondimensional total heat transfer rate (Eq. 5.3)
r	aspect ratio
R	intensity location (Figure 2.2)
S	radiation path length
T	temperature
U	x-direction velocity component
V	y-direction velocity component

W z-direction velocity component

x_i spatial coordinate in i direction

Greek Symbols

Γ nondimensional emissive power (Eq. 4.4)

δ_{ij} Kronnecker delta

ε_i emissivity of surface i

ε_g total gas emittance (Eq. 4.2)

η nondimensional optical distance

θ elevation angle ($0 \leq \theta \leq \pi$)

H nondimensional temperature (Eq. 5.2)

κ extinction coefficient

λ wavelength

σ Stefan-Boltzmann constant

σ_s scattering coefficient

τ nondimensional optical distance

τ_o optical thickness (Eq. 2.9)

ϕ azimuthal angle ($0 \leq \phi \leq 2\pi$)

Φ scattered intensity phase function

ω solid angle-scattered radiation

ω_i solid angle-incoming radiation

Ω_o scattering albedo (Eq. 2.8)

IMPLEMENTATION AND EVALUATION OF A PARTICIPATING MEDIA RADIATION MODEL IN THE TEMPEST THERMAL-HYDRAULIC COMPUTER CODE

1.0 DESCRIPTION OF PROBLEM

1.1 INTRODUCTION

The study of energy transfer through media that can absorb, emit, and scatter radiation, otherwise known as participating media radiation, has received increased attention in the past two decades. This interest stems from complicated phenomena associated with such diverse fields as rocket propulsion, combustion chambers, energy conservation, nuclear fusion, and cyrogenics. The mathematical difficulties involved in solving problems in these areas are substantial, since the basis for analyzing a radiation field in participating medium is the equation of radiative transfer (Sparrow and Cess 1978), which is an integro-differential equation written in terms of the radiative intensity. Simplifying assumptions must be made before a tractable problem is obtained.

The problem is further complicated when it is considered that most practical engineering problems do not involve radiation as the only mode of heat transfer but in combination with conduction and convection. In addition, the geometries involved in many practical problems must be modeled in three dimenisions to provide reasonable results. Therefore, a need exists for a method which will solve thermal-hydraulic problems involving participating media radiation in three dimensions.

1.2 OBJECTIVE

The objective of this study is to implement a method for solving the differential form of the radiative transfer equation into an existing three-dimensional thermal-hydraulic computer program. The results of this model for both radiative transfer and combined mode problems are then compared against analytical solutions and experimental data to determine the level of accuracy and limits to its applications. The radiative transfer equation is simplified by using a differential approximation to make it compatible with the formulation of the thermal-hydraulic code equations. The resulting expression is cast in a finite-difference form which is solved numerically. The TEMPEST computer program was selected as the base thermal-hydraulic computer code to be modified.

To accomplish the above objectives, the following chapters will be presented as two basic subsections: 1) the approximate radiative transfer equation formulation and implementation in TEMPEST, and 2) comparison of code results with existing solutions.

2.0 DEVELOPMENT OF THE SOLUTION METHOD FOR RADIANT ENERGY TRANSFER

2.1 INTRODUCTION

A description of the problem of radiative transfer in an absorbing, emitting, and scattering medium along with possible methods of solution are presented in this chapter. Included in this chapter are: 1) the development of the equation of radiative transfer, 2) a discussion of the possible approximations used to simplify the radiative transfer equation, and 3) a description of the formulation resulting from the P-1 approximation.

2.2 EQUATION OF RADIATIVE TRANSFER

The transfer of radiant energy is described in terms of radiation intensity, I_λ, which is defined as the radiation energy per unit time, per unit of projected area and per unit solid angle. The subscript λ indicates a dependency on wavelength. An equation of transfer describes the intensity of radiation at any position along its path through an absorbing, emitting and scattering medium. The derivation given here is similar to that found in Siegel and Howell (1980). Figure 2.1 illustrates the geometry used in the derivation.

As thermal radiation passes through the medium, the intensity may change due to several different effects:

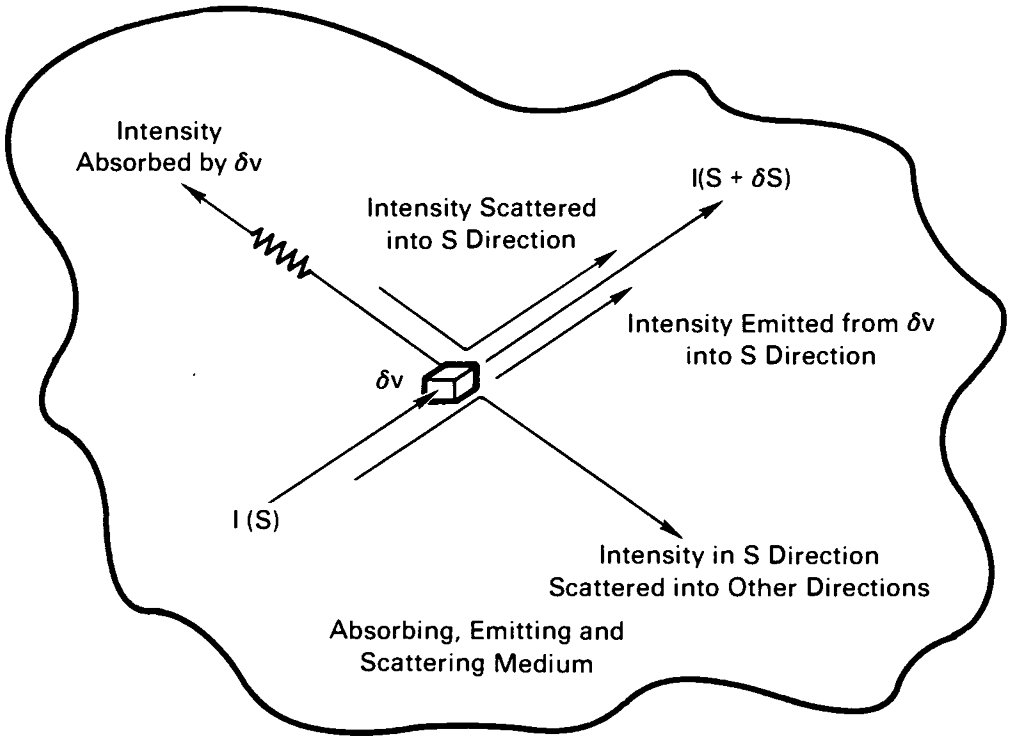

Figure 2.1. Geometry for derivation of equation of transfer

a) The intensity is reduced due to absorption of radiant energy by the medium.

b) The intensity is reduced as a result of scattering by the medium in other directions.

c) The intensity is increased because of emission of radiation from the medium.

d) The intensity is increased by energy scatterd by the medium into the direction of interest.

As radiation passes through a medium, the reduction in intensity due to absorption and scattering has been found to depend on the magnitude of the local intensity, I_λ. If a coefficient of proportionality, κ_λ, is used which is dependent on the local properties of the medium, the decrease in intensity per increment as of path length S is given by

$$dI_{\lambda\kappa} = -\kappa_\lambda(S)I_\lambda(S)dS \tag{2.1}$$

The coefficient κ_λ, also known as the extinction coefficient, is the sum of an absorption coefficient, a_λ, and a scattering coefficient, σ_s.

If the radiation is in local thermodynamic equilibrium, the spontaneous emission contribution by the medium along the path length dS to the intensity in the S direction is given by

$$dI_{\lambda e} = a_\lambda(S)I_{\lambda b}(S)dS \tag{2.2}$$

where $I_{\lambda b}$ is the black-body intensity.

The increase in intensity due to incoming scattering in direction S can be written as

$$dI_{\lambda s} = \frac{\sigma_{s\lambda} dS}{4\pi} \int_{4\pi} I_\lambda(S,\omega_i)\Phi(\lambda,\omega,\omega_i)d\omega_i \qquad (2.3)$$

where ω and ω_i are the solid angles for scattered and incoming radiation and the phase function Φ $(\lambda,\omega,\omega_i)$ has the physical interpretation of being the scattered intensity in a direction divided by the intensity that would be scattered in that direction if the scattering were isotropic.

When these terms are combined in the form of a radiant energy balance and include transient effects, the following integro-differential equation is obtained

$$\frac{1}{c}\frac{dI_\lambda}{dt} + \frac{dI_\lambda}{dS} = -\kappa_\lambda I_\lambda + a_\lambda I_{\lambda b} + \frac{\sigma_{s\lambda}}{4\pi}\int_{4\pi} I_\lambda \Phi d\omega_i \qquad (2.4)$$

For most engineering applications the complexity of this equation is prohibitive. An exact solution may require integrations with respect to time, position, wavelength, and direction. Usually, steady-state conditions may be assumed since the speed of propagation, c, is very large and the intensity field can adjust almost instantaneously for most practical problems. To further simplify the analysis, the medium properties may be assumed independent of wavelength (i.e., gray medium) and also independent of position (i.e., temperature and pressure). The radiative properties of most materials vary as a function of wavelength, therefore the gray medium assumption implies that calculated average values of these properties will adequately describe the associated physical phenomenon. In addition, it is often assumed that the scattering mechanism is isotropic. With these assumptions it is therefore obtained:

$$\begin{aligned} a_\lambda(S) &= a \\ \sigma_{s\lambda}(S) &= \sigma_s \\ \Phi(\lambda,\omega,\omega_i) &= 1.0 \end{aligned} \tag{2.5}$$

Applying these simplificatons, Equation 2.4 becomes

$$\frac{dI}{dS} = -\kappa I + aI_b + \frac{\sigma_s}{4\pi}\int_{4\pi} I d\omega_i \tag{2.6}$$

Sometimes it is more convenient to write this equation as

$$\frac{1}{\kappa}\frac{dI}{dS} = -I + (1-\Omega_0)I_b + \frac{\Omega_0}{4\pi}\int_{4\pi} I d\omega_i \tag{2.7}$$

where Ω_0 is the scattering albedo defined as

$$\Omega_0 = \sigma_s/(a + \sigma_s). \tag{2.8}$$

2.3 APPROXIMATE METHODS OF SOLUTION

As stated in Section 2.2, the equation of radiative transfer is an integro-differential equation and, therefore, exact solutions for all but the most simple problems are nearly impossible to obtain. Therefore, some additional simplifying assumptions must be made before this equation can be used to solve practical problems. Two simplifications have already been made in the derivation presented in Section 2.2, the gray-medium and steady-state assumptions. Other assumptions which may further simplify the equation are made with regard to the optical thickness of the problem or the angular distribution of the intensity within the medium.

One of the most important dimensionless parameters associated with radiation-participating medium is the optical thickness of the medium. Letting L be the characteristic physical dimension of a particular problem and κ the extinction coefficient of the medium, the optical thickness is defined as

$$\tau_o = \kappa L \tag{2.9}$$

The optical thickness is a measure of the ability of a given path length of gas to attenuate radiation.

One of the limiting cases with regard to optical thickness is the case where $\tau_o \gg 1$, also known as the optically thick or diffusion approximation. The assumption is that the optical depth of the medium is sufficiently large, and the temperature gradients sufficiently small, that the local intensity results only from local emission. In other words, every element of the medium is directly affected only by its neighbors and, as in the case of thermal conduction, the radiation transfer within the medium is assumed to be a diffusion process. More specifically, the radiation flux in a particular direction is given by the expression (Siegel and Howell 1980)

$$q_R = - \frac{4\sigma}{3\kappa} \nabla(T^4) = - \frac{4}{3\kappa} \text{ grad } e_b \tag{2.10}$$

$$e_b = \sigma T^4$$

where e_b is the black-body emissive power.

Consider the opposite extreme of $\tau_o \ll 1$ which is referred to as the optically thin approximation. The medium in this case is assumed to have such a low extinction coefficient that the intensity does not vary along a path within the field. Therefore, every element of the medium exchanges radiation directly with the bounding surfaces, such that there is no radiative interaction between adjacent elements.

For most practical problems involving participating media, the optical thickness lies in the intermediate range between these two extremes. Therefore, use of either of these assumptions would severely limit the generality of the solution method.

An alternate method for simplifying the radiative transfer equation is to assume a given angular distribution of the intensity within the medium. This assumption essentially reduces the integro-differential equation of transfer to a differential form while retaining all the terms in the equation. Typical approximations for the intensity distribution include the Milne-Eddington and Schuster-Schwarzschield approximations (Ozisk 1973), the discrete ordinate approximation (Chandrasekhar 1960), and the spherical harmonics approximation (Siegel and Howell 1980).

The Milne-Eddington and Schuster-Schwarzschield approximations divide the intensity field into hemispherical components which are each assumed to be isotropic but which may be of different magnitudes. The discrete ordinate approximation extends this method by dividing the intensity into mean components from several discrete directions. In the spherical harmonics method, the angular distribution is represented by an infinite series of spherical harmonics. The series representation is terminated after a finite number of terms depending upon the desired order of approximation.

The method chosen for this study to simplify the integro-differential Equation 2.7 is to specify the angular distribution of intensity using the spherical harmonies method. Experience has shown that the spherical-harmonics method can produce reasonably accurate results with a relatively simple solution procedure (Siegel and Howell 1980; Ratzel 1981; and Bayazitoglu and Hiegenyi 1979).

2.4 FORMULATION OF THE P-1 APPROXIMATION

The equation for radiant energy transfer derived in Section 2.2 is

$$\frac{1}{\kappa}\frac{dI}{dS} = - I + (1-\Omega_o)\ I_b + \frac{\Omega_o}{4\pi}\int_{4\pi} I d\omega_i \tag{2.7}$$

The total derivative for the direction R can be transformed into three orothogonal spatial components for a three-dimensional representation using the expression

$$d/dR = \hat{\ell}_1\ \partial/\partial x_1 + \hat{\ell}_2\ \partial/\partial x_2 + \hat{\ell}_3\ \partial/\partial x_3 \tag{2.11}$$

where x_1, x_2, x_3 are the coordinate directions and $\hat{\ell}_1$, $\hat{\ell}_2$, $\hat{\ell}_3$ are the direction cosines.

For instance, in a Cartesian system this would be

$$d/dR = \cos\Theta\ \partial/\partial x_1 + \sin\Theta\cos\phi\ \partial/\partial x_2 + \sin\Theta\ \sin\phi\ \partial/\partial x_3 \tag{2.12}$$

where the direction cosines are defined in Figure 2.2.

Using this notation, Equation 2.7 becomes

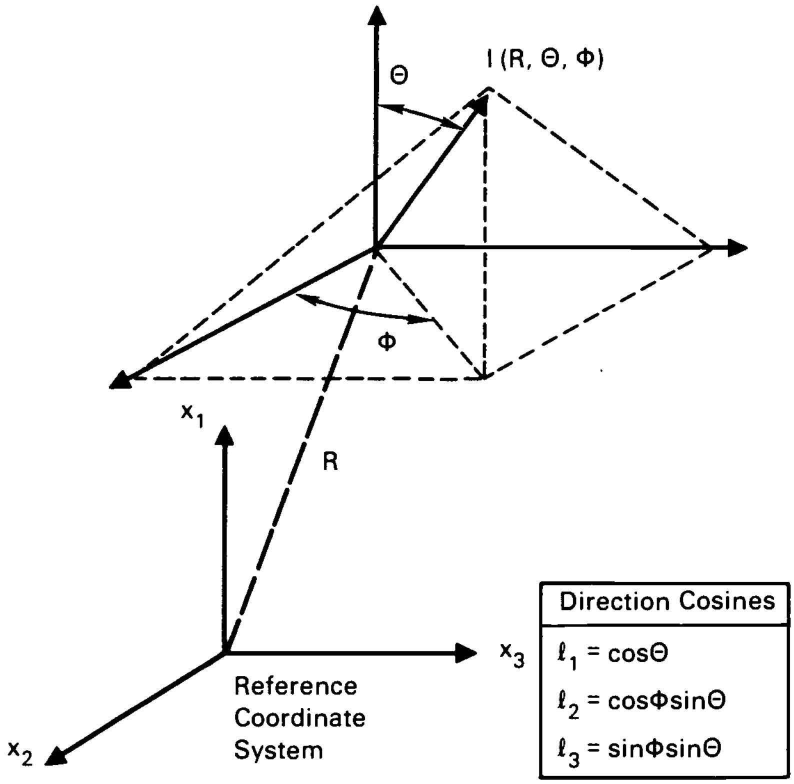

Figure 2.2. Cartesian coordinate system and direction cosines

$$\sum_{i=1}^{3} \hat{\ell}_i \, \partial I/\partial x_i + I = (1-\Omega_0)\, I_b + \Omega_0/4\pi \int_{4\pi} I d\omega_i \qquad (2.13)$$

with $I = I(R,\Theta,\phi)$, $I_b = I_b(R)$.

An expression for the angular distribution of intensity is required to solve Equation 2.13. In the spherical harmonics expansion technique used here the intensity distribution is expanded in an orthogonal series of spherical harmonics of the form:

$$I(R,\Theta,\phi) = \sum_{n=0}^{\infty} \sum_{m=-n}^{n} A_n^m(R) Y_n^m(\Theta,\phi) \tag{2.14}$$

where $A_n^m(R)$ are a set of position dependent coefficients and $Y_n^m(\Theta,\phi)$ are the normalized spherical harmonics given by

$$Y_n^m(\Theta,\phi) = \left[\frac{2n+1}{4\pi} \frac{(n-m)!}{(n+m)!}\right]^{1/2} e^{jm\phi} P_n^m(\cos\Theta) \tag{2.15}$$

The $P_n^m(\cos\Theta)$ are the associated Legendre polynominals of the first kind (Wylie 1960), defined by

$$P_n^m(\cos\Theta) = \frac{2^{m+1}}{\pi^{1/2}} (\sin\Theta)^m \frac{\Gamma(n+m+1)}{\Gamma(n+3/2)} \sum_{k=0}^{\infty} \{\frac{(m+1/2)k(n+m+1)k}{k^0(n+3/2)k}$$

$$* \sin[(n+m+2k+1)\Theta]\} \tag{2.16}$$

where $\Gamma(\zeta)$ is the gamma function, and the notation $(\alpha)_k$ is Pochhammer's symbol

$$(\alpha)_0 = 1 \qquad \alpha \neq 0$$

$$(\alpha)_k = \alpha(\alpha+1)(\alpha+2)\ldots(\alpha+k-1).$$

Table 2.1 defines the associated Legendre polynominal expressions for positive n=0 through n=3.

Since the expression for the angular distribution of intensity is an infinite series, it must be truncated after a finite number of terms to obtain a usuable expression. The P-N approximation follows when one terminates the series such that:

$$A_n^m(R) = 0 \text{ for } n > N \tag{2.17}$$

In the limit as $n \to \infty$, the P-N representation for the intensity becomes exact. However, for practial problems, the number of terms in the expansion multiplies dramatically with increasing N so that a small value for N is required to obtain a manageable expression. As discussed in Chapter 1, work in the field of radiant energy transfer has generally involved the P-1 and P-3 approximations. The even P-N approximations have not been used because of the difficulty in obtaining usable boundary conditions (Marshak 1946).

Table 2.1. Associated Legendre Polynominals

(P_n^m (cos θ)

n	m=0	m=1	m=2	m=3
0	1.0	-	-	-
1	$\cos\Theta$	$\sin\Theta$	-	-
2	$\frac{3\cos^2\Theta - 1}{2}$	$3\cos\Theta\sin\Theta$	$3\sin^2\Theta$	-
3	$\frac{5\cos^3\Theta - 3\cos\Theta}{2}$	$\frac{3}{2}(5\cos^2\Theta - 1)\sin\Theta$	$15\cos\Theta\sin^2\Theta$	$15\sin^3\Theta$

The amount of computational effort required and the complexity of the numerical formulation are strongly dependent on the P-N approximation selected. If the P-1 approximation is selected, the solution of one second-order differential equation with the appropriate boundary conditions is required. If the P-3 approximation is selected, four coupled second-order differential equations with more complex boundary conditions must be solved simultaneously. This model will be used primarily to calculate the contribution of radiant heat transfer to problems where conduction and convection heat transfer modes are dominant, and computational speed is an important consideration. The P-1 approximation was therefore selected. With this approximation, the radiative intensity is assumed to have an angular distribution of the form

$$I(R,\Theta,\phi) = \frac{1}{2\sqrt{\pi}} [A_0^0 + \sqrt{3}A_1^0 \cos\Theta - \sqrt{3/2} \sin\Theta \; (A_1^1 - A_1^{-1}) \cos\phi$$

$$+ j \; (A_1^1 + A_1^{-1} \sin\phi)] \tag{2.18}$$

where $A_n^m(R)$ are the coefficients expressed as functions of position.

In applying the P-1 intensity distribution it is useful to express the spatially dependent coefficients $A_n^m(R)$ in terms of moments of intensity. This is achieved by multiplying both sides of Equation 2.18 by powers of the direction cosines ($\hat{\ell}_i$, i=1, 2, 3) individually or in a combination and integrating the resulting expression over a solid angle of 4π. The moments are defined as follows:

$$I_0(R) = \int_{\omega=4\pi} I(R,\omega) d\omega \tag{2.19}$$

$$I_i(R) = \int_{\omega=4\pi} \hat{\ell}_i \, I(R,\omega) d\omega \qquad (i=1,2,3) \qquad (2.20)$$

$$I_{ij}(R) = \int_{\omega=4\pi} \hat{\ell}_i \hat{\ell}_j \, I(R,\omega) d\omega \qquad (i,j=1,2,3) \qquad (2.21)$$

$$\vdots$$

$$I_{ij\ldots\kappa}(R) = \int_{\omega=4\pi} \hat{\ell}_i \hat{\ell}_j \ldots \hat{\ell}_\kappa \, I(R,\omega) d\omega \quad (i,j\ldots\kappa=1,2,3) \qquad (2.22)$$

The change from using coefficients A_n^m to moments of intensity is made because the first three types of moments have physical significance. The zeroth order moment, $I_0(R)$, divided by the speed of light, gives the radiation energy density. The first moments, $I_i(R)$, are the radiative fluxes in the i coordinate directions. The second moments, $I_{ij}(R)$, divided by the speed of light, comprise the radiation stress and pressure tensor, analogous to the elements of the stress tensor in fluid dynamics (Siegel and Howell, 1980). The higher order moments have no specific physical significant and are generated by analogy with the first three.

The relationships between the coefficients A_n^m and the moments of intensity are obtained by substituting Equation 2.18 into the expressions defining the moments of intensity and integrating. This procedure is described in Appendix A. The resulting expression for intensity in terms of moments is

$$I(R,\Theta,\phi) = 1/4\pi\ [I_0+3I_1\cos\Theta+3I_2\sin\Theta\ \cos\phi + 3I_3\sin\Theta\sin\phi] \qquad (2.23)$$

The equation of transfer is transformed into a series of partial differential equations in terms of the moments by multiplying the equation of radiant transfer (Equation 2.13) by powers of the direction cosines ($\hat{\ell}_i$, i=1,2,3) and integrating over all solid angles ω. By simply integrating Equation 2.13 and noting that I_b is independent of angle, the definitions for I_0 and I_i are used to obtain

$$\sum_{i=1}^{3} \partial I_i/\partial x_i = a\ [4\pi I_b - I_0] \qquad (2.24)$$

Multiplying Equation 2.13 by $\hat{\ell}_i$(j=1,2,3) and integrating gives the first-order moment equation

$$\sum_{i=1}^{3} \int_{4\pi} \hat{\ell}_j \hat{\ell}_i \partial I/\partial x_i d\omega = a \, [I_b \int_{4\pi} \hat{\ell}_j I d\omega] \tag{2.25}$$

which can be written as

$$\sum_{i=1}^{3} \partial I_{ij}(R)/\partial x_i = -a \; I_j(R) \qquad j=1,2,3 \tag{2.26}$$

This procedure is continued to generate, for example, the nth order moment equation of the form

$$\sum_{i=1}^{3} \frac{\partial I_{k^n i}(R)}{\partial x_i} = -a \; I_k{}^n(R) \qquad k=1,2,3 \tag{2.27}$$

By continuing the process an infinite set of moment equations can be generated as $n \to \infty$.

The next step is to approximate the infinite set of moment equations by a finite set. When such a truncation is carried out, there will in general be fewer equations than unknowns. The governing equations for the P-1 approximation are

$$\partial I_1/\partial x_1 + \partial I_2/\partial x_2 + \partial I_3/\partial x_3 = a\,[4\pi I_b - I_o] \tag{2.28}$$

$$\partial I_{11}/\partial x_1 + \partial I_{21}/\partial x_2 + \partial I_{31}/\partial x_3 = -\kappa I_1 \tag{2.29}$$

$$\partial I_{12}/\partial x_1 + \partial I_{22}/\partial x_2 + \partial I_{32}/\partial x_3 = -\kappa I_2 \tag{2.30}$$

$$\partial I_{13}/\partial x_1 + \partial I_{23}/\partial x_2 + \partial I_{33}/\partial x_3 = -\kappa I_3 \tag{2.31}$$

To close the set of equations, the expression for intensity in terms of A_n^m is substituted into the first three moment equations to give

$$I_o = 2\sqrt{\pi}\, A_o^o \tag{2.32}$$

$$I_{ij} = 2/3\, \sqrt{\pi}\, A_o^o\, \delta_{ij} \tag{2.33}$$

where δ_{ij} is the Kronecker delta. Eliminating A_o^o by combining the two expressions gives the closure condition

$$I_{ij} = 1/3\ \delta_{ij} I_o \qquad 2.34$$

When the closure condition is applied to the governing Equations 2.28 through 2.31, the equations simplify the four first-order partial differential expressions in terms of I_o, I_1, I_2, and I_3.

$$\partial I_1/\partial x_1 + \partial I_2/\partial x_2 + \partial I_3/\partial x_3 = a\ [4\pi I_b - I_o] \qquad (2.35)$$

$$I_1 = 1/3\kappa\ \partial I_o/\partial x_1 \qquad (2.36)$$

$$I_2 = 1/3\kappa\ \partial I_o/\partial x_2 \qquad (2.37)$$

$$I_3 = 1/3\kappa\ \partial I_o/\partial x_3 \qquad (2.38)$$

Note that the radiative heat transfer in the x_1, x_2, and x_3 directions are defined by Equations 2.36 through 3.38.

A single second-order partial differential expression in terms of I_o is obtained by substituting Equations 2.36-38 into Equation 2.35 to obtain

$$\frac{1}{3\kappa}\left[\frac{\partial^2 I_o}{\partial x_1^2} + \frac{\partial^2 I_o}{\partial x_2^2} + \frac{\partial^2 I_o}{\partial x_3^2}\right] = -a\left[4\pi I_b - I_o\right] \tag{2.39}$$

This equation is specifically for the Cartesian coordinate system. If vector notation is used the equation takes the general form

$$1/3\kappa\nabla^2 I_o = -a\left[4\pi I_b - I_o\right] \tag{2.40}$$

This equation is the approximate form of the radiant transfer equation applicable to participating media, simplified using the P-1 approximation.

Solution of Equation 2.40 requires a set of appropriate boundary conditions. Several approaches have been developed to obtain boundary conditions for the spherical harmonics method (Davison 1958). The method chosen was proposed by Marshak (1946), who suggested that the exact boundary condition should be satisfied in an integral sense.

The appropriate boundary conditions are derived by considering a gray boundary A_j that is perpendicular to the x_j direction as shown in Figure 2.3. The net radiative energy leaving A_j in the positive x_j direction is

$$\begin{aligned} q_w &= \varepsilon_j \sigma T_j^4 + (1-\varepsilon_j) q_i - q_i \\ &= \varepsilon_j \pi I_b - \varepsilon_j q_i \end{aligned} \tag{2.41}$$

that is, the sum of the emitted energy plus the reflected energy minus the incoming flux, q_i. to use this expression the incoming flux must be expressed in terms of intensity or its moments. This is done using the expression

$$q_i = \int I \hat{\ell}_j d\omega \tag{2.42}$$

where $\hat{\ell}_j$ is the cosine of the angle between I and the x_j direction.

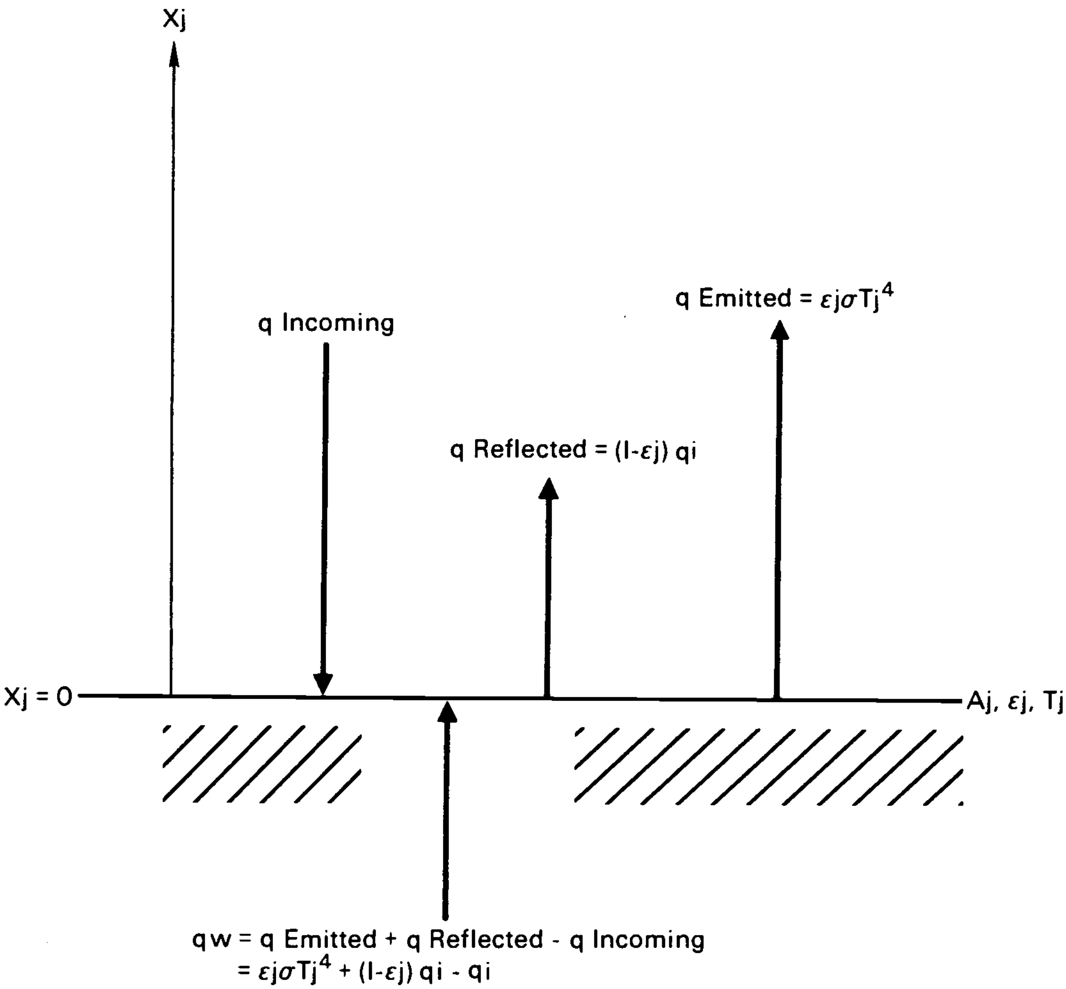

Figure 2.3. Coordinate system showing heat fluxes in the boundary condition

The expression for the intensity in terms of its moments is

$$I = 1/4\pi\ [I_0 + 3I_1\cos\Theta + 3I_2\sin\Theta\cos\phi + 3I_3\sin\Theta\sin\phi] \quad (2.23)$$

As an example, assume the boundary surface is normal to the x_1 direction. The integral expression for q_i then becomes

$$q_i = \iint \frac{1}{4\pi} [I_o + 3I_1\cos\Theta + 3I_2\sin\Theta\cos\phi + 3I_3\sin\Theta\sin\phi] \cos\Theta\sin\Theta d\Theta d\phi$$

$$= \frac{I_o}{4} - \frac{I_1}{2} \qquad (2.43)$$

Substituting this into Equation 2.41 yields

$$q_w = \varepsilon_j\pi I_b - \varepsilon_j [I_o/4 - I_1/2]$$

$$= \varepsilon_j\pi [I_b - I_o/4\pi] + \varepsilon_j I_1/2 \qquad (2.44)$$

Recall that I_1 is defined as the radiative flux in the x_1 direction. Therefore

$$q_w = \varepsilon_j \pi \, [I_b - I_o/4\pi] + \varepsilon_j q_w/2$$

$$q_w \, [1 - \varepsilon_j/2] = \varepsilon_j \pi \, [I_b - I_o/4\pi]$$

$$q_w = \frac{2\varepsilon_j \pi}{2-\varepsilon_j} [I_b - I_o/4\pi] \qquad (2.45)$$

$$= \frac{\varepsilon_j}{2(2-\varepsilon_j)} [4\pi I_b - I_o]$$

Note that the boundary condition is stated in terms of the first moment of intensity, I_o, and is therefore compatible with the approximate form of the radiant transfer equation (Equation 2.40).

3.0 IMPLEMENTATION OF THE RADIATION MODEL

3.1 INTRODUCTION

This chapter describes the implementation of the radiation model derived in Chapter 2 into a three-dimensional thermal-hydraulic computer code. Included in this chapter are: 1) a description of the TEMPEST computer code, 2) a derivation of the numerical equations used to represent the radiation model and 3) a description of the numerical methods used to solve the equations.

3.2 A BRIEF DESCRIPTION OF THE TEMPEST CODE

3.2.1 General Description

The computer program which was selected to incorporate the participating medium radiation model was the TEMPEST[a] code (Trent, Eyler and Budden, 1983), developed by the Pacific Northwest Laboratory for the U.S. Department of Energy. TEMPEST is a transient, three-dimensional, hydrothermal computer program that is designed to analyze a broad range of coupled fluid dynamic and heat transfer problems. The equations governing mass, momentum, and energy conservation are solved using finite-difference techniques. Analysis may be conducted in either cylindrical or Cartesian coordinate systems. The TEMPEST

(a) Transient Energy, Momentum and Pressure Equation Solution in Three dimensions cylindrical or Cartesian coordinate systems. The TEMPEST technical approach is based on techniques standard to computational fluid mechanics; however, it contains the unique feature of fully coupled hydrodynamic and solid material heat diffusion solutions. The energy equation is treated implicitly in time using an implicit continuation procedure, and the code can be used specifically to solve heat conduction problems.

A large amount of testing, assessment, and validation has been conducted using TEMPEST, which was performed to assure that solution logical procedures are working correctly and that the physics are modeled properly (Eyler, Trent and Budden, 1983). This work represents an extensive assessment and validation of the TEMPEST code.

Because TEMPEST is structured with considerable generality, is user oriented, and is applicable to a wide range of hydrothermal problems, it is a valuable hydrothermal design analysis tool for many areas of practical interest. However, the usefulness of the TEMPEST code would be considerably enhanced with the addition of a general thermal radiation model.

3.2.2 Description of the Energy Solution

The equation used in the TEMPEST code to describe the conservation of thermal energy for incompressible flow is:

$$\rho_o c \left[\frac{\partial T}{\partial t} + \frac{1}{R^\beta}\frac{\partial}{\partial R}(R^\beta UT) + \frac{1}{R^\beta}\frac{\partial}{\partial X}(WT) + \frac{\partial}{\partial Z}(VT)\right]$$

$$= \frac{1}{R^\beta}\frac{\partial}{\partial R}\left(\sigma R^\beta \frac{\partial T}{\partial R}\right) + \frac{1}{R^{2\beta}}\frac{\partial}{\partial X}\left(\sigma \frac{\partial T}{\partial Z}\right) + \frac{\partial}{\partial Z}\left(\sigma \frac{\partial T}{\partial Z}\right) + \dot{Q}$$

where

$\sigma = k + k_T$

k = thermal conductivity

k_T = turbulent (eddy) thermal conductivity

c = specific heat

$\dot{Q}$ = volumetric heat generation rate

U,V,W = velocity components in the x, y, and z directions

β = 1 for cylindrical coordinates

β = 0 for Cartesian coordinates

Since this equation and all the other scalar transport equations have the same form, a general solution procedure is developed and implemented in TEMPEST. The method chosen to solve these equations is the Douglas and Gunn three-step algorithm (Douglas and Gunn, 1964).

The expression derived in Chapter 2 to describe the transport of radiant energy was formed in terms of radiation intensity and its moments. Since the intensity has units of temperature to the fourth power and the thermal energy equation is expressed simply in terms of temperature, an implicit treatment of the radiant energy absorbed by the fluid is not possible. Therefore, a separate solution of the radiant energy equation is performed sequentially with the thermal energy equation using the most recent fluid temperature field. The resulting energy absorbed by the fluid in each cell is then explicitly added to the source term, $\dot{Q}$, of the thermal energy equation before proceeding further with the thermal solution.

3.3 IMPLEMENTATION OF THE SOLUTION METHOD

3.3.1 Description of the Numerical Equations

As mentioned before, the equations which are numerically solved in the TEMPEST code are cast in a finite-difference form. For the two solutions to be fully compatible, the differential equation derived to represent the transfer of radiant energy in participating medium must be expressed using similar differencing procedures. The same is also true for the boundary conditions. Recall that the final equation derived in Chapter 2 was

$$1/3\kappa\nabla^2 I_o = -a\ [4\pi I_b - I_o] \qquad (2.40)$$

where I_o is the zeroth-order moment of the intensity.

Remember also that the first moments, I_i, are the radiative fluxes in the i coordinate direction, and are related to I_0 by the expressions

$$I_i = -1/3\kappa \; \partial I_0/\partial x_i = -1/3\kappa \nabla I_0$$

(2.36-38)

Note that Equation 3.1 is simply a form of Poisson's equation, which describes a diffusion process with a source term. A familiar analogy would be that of energy transport by means of thermal conduction,

$$q = - k\nabla T \tag{3.2}$$

The temperature gradient in Equation 3.2 is replaced in Equation 2.36 by the spatial derivative of I_0 as the driving force and the thermal conductivity, k, is replaced by the term $1/3\kappa$. This is significant because extensive effort has gone into the development of conventional numerical solution schemes for problems of this form in three dimensions.

To derive numerical equations representing this differential equation, the medium of a particular problem is divided into a finite number of control volumes or cells. An example of such a cell in the Cartesian coordinate system is shown in Figure 3.1. A radiant energy balance is performed on the cell and the derivatives in each term are replaced by finite-difference formulations. For example, the amount of radiant energy leaving the face of the cell in the positive x-direction is

$$Q_x = dA = dydz \left[\frac{1}{3\kappa} \frac{\partial I_o}{\partial x}\right] \tag{3.3}$$

The derivative is replaced by

$$\frac{\partial I_o}{\partial x} = \frac{[I_{o\ i+1} - I_{o\ i}]}{1/2\ [\Delta x_{i+1} + \Delta x_i]} \tag{3.4}$$

therefore

$$Q_x = \frac{2}{3k} \frac{\Delta y \Delta z}{[\Delta x_{i+1} + \Delta x_i]} [I_{o\ i+1} - I_{o\ i}] \tag{3.5}$$

$$= K_i\ [I_{o\ i+1} - I_{o\ i}]$$

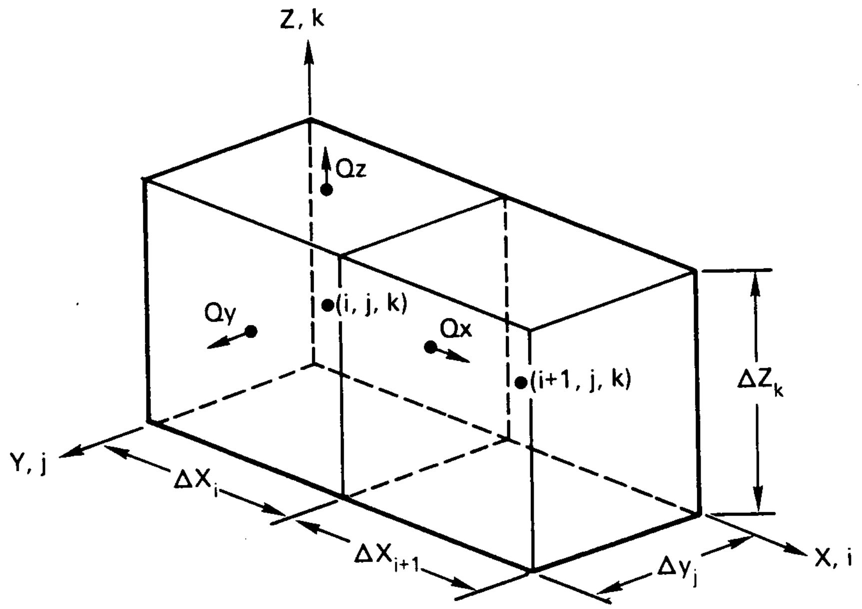

Figure 3.1. Computational cell in the Cartesian coordinate system

where

$$K_i = \frac{2}{3\kappa} \frac{\Delta y \Delta z}{[\Delta x_{i+1} + \Delta x_i]}$$

Equivalent expressions can be derived in the y and z directions.

A separate expression is required when the medium cell is bounded by a wall cell. Recall that the new radiative energy flux leaving a particular wall is given by the expression

$$q_w = \frac{\varepsilon_j}{2(2-\varepsilon_j)} [4\pi I_b - I_o^*] \qquad (2.45)$$

where I_o^* is the value of the first moment of intensity immediately adjacent to the wall. In this case, there is no derivative to be represented and the expression is analogous to a wall heat transfer coefficient. To calculate the total heat entering the cell from the wall, the radiative resistance from the cell boundary to the centerpoint must be accounted for. Therefore,

$$Q_x = \frac{\Delta y \Delta z \varepsilon_j}{2(2-\varepsilon_j)} [4\pi I_b - I_o^*]$$

$$= H_i^* [4\pi I_b - I_o^*] \tag{3.6}$$

where

$$H_i^* = \frac{\Delta y \Delta z \varepsilon_j}{2(z-\varepsilon_j)}$$

$$Q_x = \frac{2\Delta y \Delta z}{3\kappa \ \Delta x_i} [I_o^* - I_o]$$

$$= K_i^* [I_o^* - I_o] \tag{3.7}$$

where

$$K_i^* = \frac{2\Delta y \Delta z}{3\kappa \Delta x_i}$$

Combining Equations 3.6 and 3.7 we obtain:

$$Q_x = K_i \,[4\pi I_b - I_o] \tag{3.8}$$

where

$$K_i = \left[\frac{1}{H_i^*} + \frac{1}{K_i^*}\right]^{-1}$$

$$= \Delta y \Delta z \left[\frac{3\kappa \Delta x_i}{2} + \frac{2(2-\varepsilon_j)}{\varepsilon_j}\right]^{-1}$$

The source term in the equation has the form

$$q_A''' = -a \,[4\pi I_b - I_o] \tag{3.9}$$

where a is the absorption coefficient and I_b is the blackbody intensity of the medium. This term represent the volumetric rate of radiant energy absorbed by the medium and converted into thermal energy. Therefore, this is the connection between the radiant energy solution and the subsequent thermal energy solution for the medium. The amount of radiant energy absorbed, as calculated by this term, is added to the source term of the energy equation before solving. If the absorption coefficient is zero, the two equations are independent for the participating medium portion of the problem. The total amount of radiant energy absorbed by a cell is given by the expression

$$Q_A = q_A''' V = a\,[4\pi I_b - I_o]\,\Delta x \Delta y \Delta z \tag{3.10}$$

$$= K_A\,[4\pi I_b - I_o]$$

where

$K_A = a\,\Delta x \Delta y \Delta z$

When a radiant heat balance is performed on each participating medium cell, a set of n linear equations are obtained, where n is the number of cells in the medium. These equations may be expressed in the matrix form

$$[K]\{I_o\} = \{S\} \tag{3.11}$$

where [K] represents the radiant energy connections and {S} includes all the terms involving the blackbody intensity, I_b.

3.3.2 Solution Procedure

The solution to the P-1 form of the radiant transfer equation is performed in subroutine PRAD, specifically designed for the TEMPEST code. A flowchart of subroutine PRAD is shown in Figure 3.2. The subroutine can be divided into three sections.

a) setting up the matrix equation (Equation 3.11)

b) solution of the equation to obtain the $[I_0]$ array

c) calculation of the source term contributions to the thermal energy equation

In the first section Equations 3.5, 3.8, and 3.10 are used to set up the matrix equation

$$[K]\{I_0\} = \{S\} \tag{3.11}$$

Unless temperature dependent radiation properties are used, the array [K] will remain constant for a particular problem. The array {S}, however, is highly temperature dependent and must be recomputed each time the thermal solution is updated. The

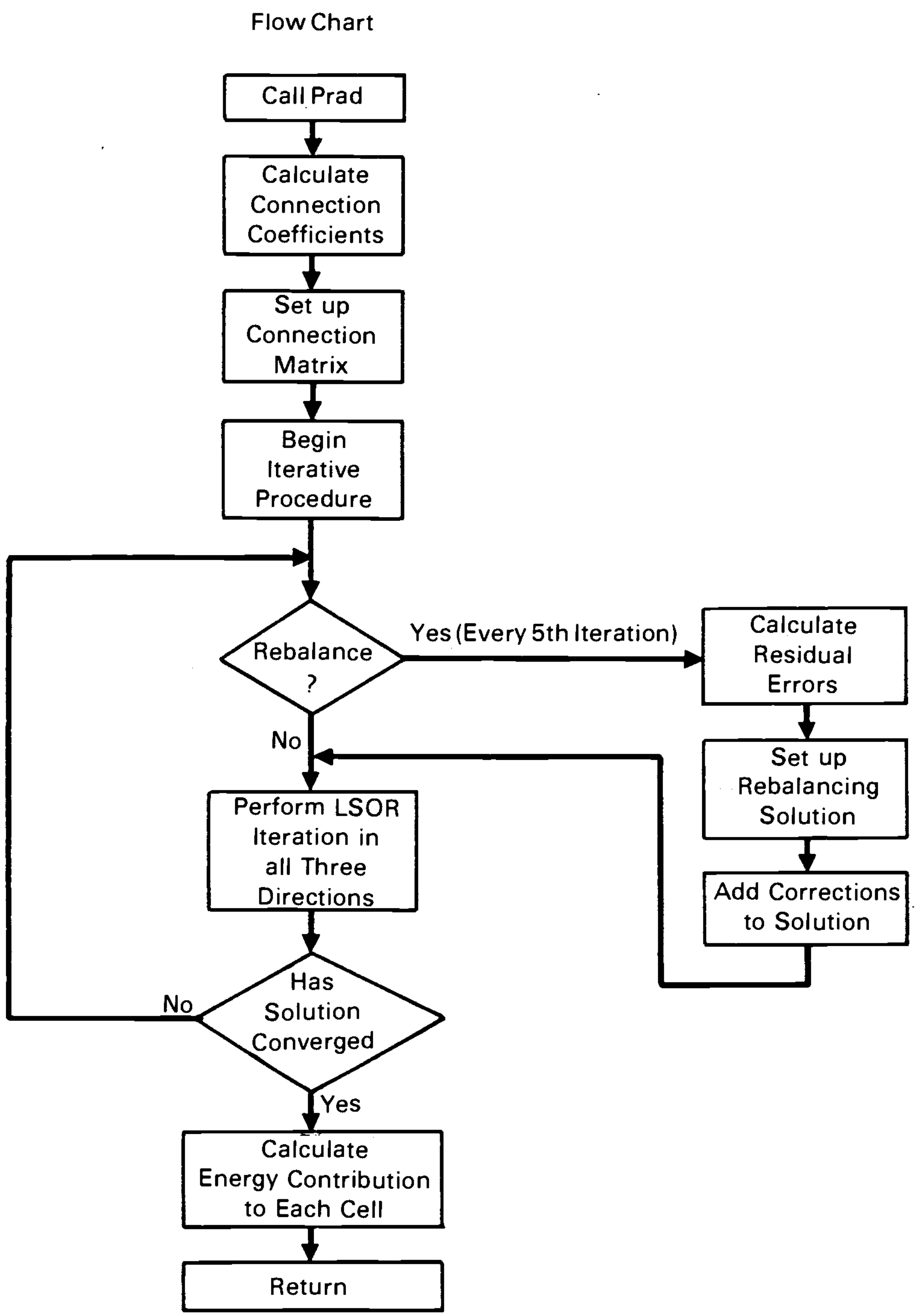

Figure 3.2. Flowchart for Subroutine PRAD

subroutine has the capability of setting up the problem in both Cartesian and cylindrical coordinate systems.

As mentioned earlier, one attractive feature of the P-1 approximation radiation model is that the resulting governing equation takes the form of Poisson's equation. For a problem in three dimensions, this equation may be solved by several different numerical methods. A description of some of these methods is found in Trent and Welty (1974). The numerical solution procedure selected for use in subroutine PRAD is the line successive overrelaxation (LSOR) method (Ames 1977). The LSOR method proceeds by dividing the region of interest into lines pointing in one direction. Each line is solved for separately using a tridiagonal matrix. The region is then divided into lines in another coordinate direction and solving as before. One iteration consists of completing this procedure in all three coordinate directions. For this reason, the LSOR method is designated as an alternating direction implicit (ADI) method. The acceleration factor selected for use in PRAD is 1.20.

Once the problem has converged, the array $\{I_0\}$ is used to calculate the source term contributions to the thermal energy equation. The radiant energy absorbed by each fluid cell is calculated using Equation 3.10. The energy transfer at the boundary wall cells is calculated using Equation 3.8.

4.0 EVALUATION: RADIANT ENERGY TRANSFER

4.1 INTRODUCTION

In Chapter 2 a method was developed which represents radiant heat transfer in a participating medium. Chapter 3 describes how this model was incorporated into a three-dimensional thermal-hydraulic computer code. To determine the accuracy and the limits of this model, a comparison must be made between the results and existing analytical solutions or experimental data. In Chapter 4 this is done for the case of pure radiation. In Chapter 5 the effectiveness of the model is evaluated for the combined modes of radiation and conduction heat transfer. In Chapter 6 the model is evaluated for radiation, conduction and convection heat transfer.

4.2 REVIEW OF LITERATURE

A great deal of literature exists in the area of thermal radiative equilibirum. The term equilibrium indicates that energy is not being absorbed by the medium and the equation of radiant transfer is, therefore, independent of the thermal energy solution. The simplest problem which may be considered is the calculation of heat transfer and temperature distribution between infinite parallel gray plates at different temperatures separated by a participating gray gas. One of the first solutions of this problem was obtained by Viskanta and Grosh (1961) using the method of undetermined parameters. The problem was also solved by numerical integration of the basic equation by Usiskin and Sparrow (1960), but was limited to black walls and values of optical thickness less than two. The case for gray walls and moderate to large optical thickness was treated by Deissler (1964) using a modified diffusion approximation with jump boundary conditions. In all these cases the analysis involved some approximations and limitations which render them inexact. A procedure developed by Heaslet and Warming (1965) showed that the solutions may be expressed in terms of functions that had previously been tabulated to a considerable degree of accuracy and may be considered exact. Therefore, the results of this analytical solution will be used for comparison. It should be noted that a numerical solution procedure using a Monte Carlo technique was developed by Howell and Perlmutter (1964) that gives results which compare very well with that of Heaslet and Warming.

Another problem which is of interest is the calculation of heat transfer and temperature distribution between infinite concentric gray cylinders separated by a gray gas. This problem was treated by Deissler (1964) using the diffusion approximation with a jump boundary condition. Beyond this, very few analytical approaches have been attempted and no exact analytical solution has been obtained due to the complexity of the problem. However, numerical solutions for this problem have been obtained by Perlmutter and Howell (1964) using a Monte Carlo solution. Although the results may not be considered exact, the accuracy of these calculations are such that they may be used as a standard against which other results may be compared. For example, results from a similar Monte Carlo solution for the parallel plate case compare very well with the exact solution (Howell and Perlmutter, 1964).

A modest amount of work has been done in the area of two-dimensional radiant energy transfer. The major portion of this work is concerned with a two-dimensional rectangular enclosure containing a gray participating gas. Glatt and Olfe (1973) calculated temperature distributions in a rectangular enclosure bounded by black walls using a modified moment method, and compared results with those obtained by Hottel's zonal method. Modest (1975) used the differential approximation as the basis for his work and applied geometry correction factors to improve boundary and medium-to-medium exchange effects for optically thin geometries. Despite the fact that the work by Modest is not an exact solution, comparison with detailed numerical solutions using Hottel's zone method indicates that the results are accurate enough to be used for comparison.

Before a radiant energy transfer problem is characterized, the values for two material properties, the scattering coefficient, σ_s, and the absorbtion coefficient, a, must be specified. As mentioned in Chapter 2, these quantities are generally functions of wavelength, λ. Therefore, some method must be used to calculate a mean value which will adequately represent the property for all wavelengths. For example, the absorption coefficient, a_λ, is extrapolated from gas emittance data using the expression

$$a_\lambda = \frac{1}{2} \left[\frac{\varepsilon_{g\lambda}}{L}\right]_{L \to 0} \qquad (4.1)$$

where L is the media slab thickness. A total gas emittance, ε_g, is calculated by

$$\varepsilon_g = \frac{\int_0^\infty \varepsilon_{g\lambda} \, e_{b\lambda} \, dx}{e_b} \qquad (4.2)$$

The Planck mean absorbtion coefficient, a_p, is then calculated using the expression

$$a_p = \frac{1}{2} \left[\frac{\varepsilon_g}{L}\right]_{L \to 0} \qquad (4.3)$$

Some representative values of a_p are illustrated in Figure 4.1 for carbon dioxide, water and carbon monoxide. The data was taken from Tien and Abu-Romia (Sparrow and Cess 1978).

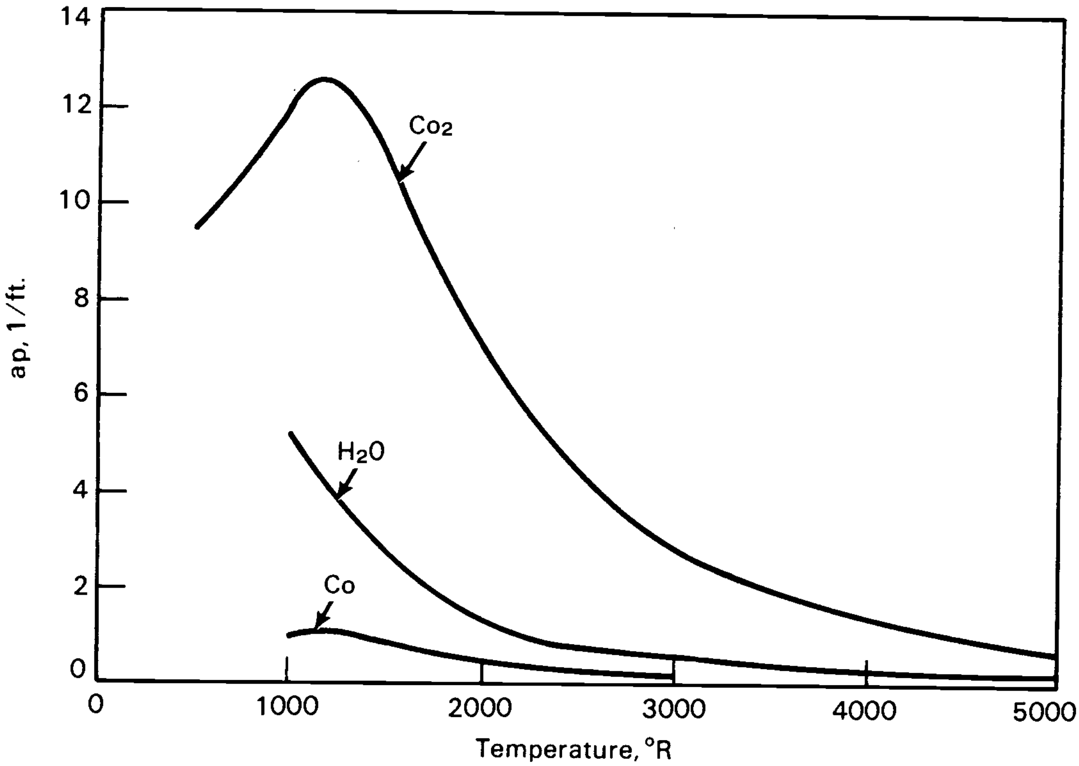

Figure 4.1. Planck mean absorption coefficients at one atmosphere pressure for carbon dioxide, water, and carbon monoxide

4.3 EVALUATION OF RESULTS

4.3.1 One-Dimensional Geometries

The first case considered is the calculation of heat transfer and emissive power distribution between infinite parallel gray plates at different temperatures. Nondimensional parameters will be used to represent both the emissive powers and heat transfer rates. The emissive powers will be represented by the parameter, Γ, which is defined as

$$\Gamma(\tau) = \frac{e_{b(\tau)} - e_{b2}}{e_{b1} - e_{b2}} \tag{4.4}$$

where e_{b1} and e_{b2} are the black body emissive powers of the hot and cold walls, respectively, and τ is the dimensionless distance in terms of optical length. The heat transfer rate is represented by the parameter, Q_R, which is defined as

$$Q_R = \frac{q_r}{e_{b1} - e_{b2}} \tag{4.5}$$

where q_r is the radiation heat transfer rate.

A comparison of nondimensional emissive power distributions from Heaslet and Warming (1965) and the P-1 approximation are presented in Figure 4.2 for different optical thicknesses. The results from Heaslet and Warming were obtained by solving two uncoupled integral equations for the temperature distributions and radiative transfer by means of tabulated functions used by Chandrasekhar (1960). Results from these studies predict the emissive power distributions near the walls more accurately than do numerical techniques.

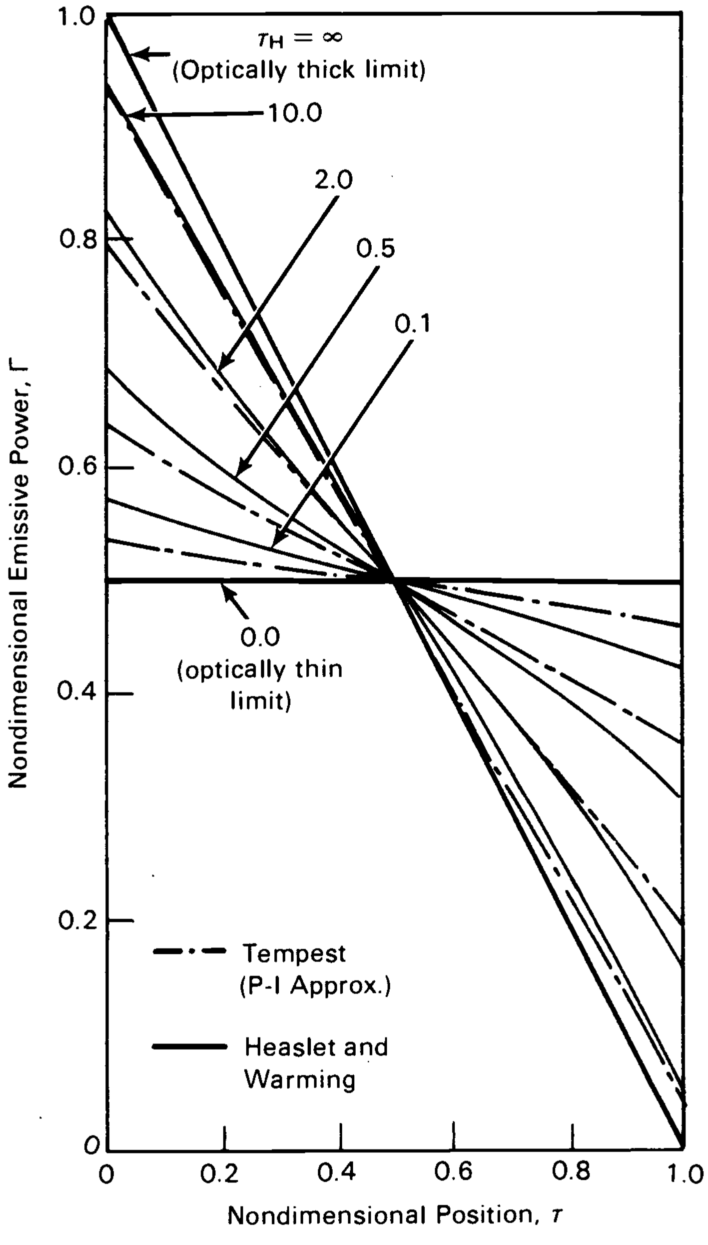

Figure 4.2. Nondimensional emissive power distributions in a planar geometry for different optical thicknesses ($\varepsilon_1 = \varepsilon_2 = 1.0$)

The calculated emissive power distributions exhibit a discontinuity between the wall temperature and the medium temperature at the wall. This discontinuity, known as the "slip" condition, is a result of the heat transfer boundary condition at the wall. Recall that in Chapter 3 the boundary condition which was derived included a term similar to a heat transfer coefficient in the thermal conduction analogy. As the optical thickness approaches zero, the emissive power becomes flat with a value equal to the arithmetic average of the wall emissive powers. For this case, the boundary condition terms dominate the problem. For large optical thicknesses, the slip condition is reduced and a linear conduction-like solution for the emissive power distribution is obtained.

Figure 4.2 shows that the ability of the P-1 approximation to predict the emissive power distribution is strongly dependent on the optical thickness. As the medium becomes optically thick, the P-1 approximation results approach the Heaslet and Warming solutions. For an optically thin medium ($\tau_0 < 1.0$), the results deviate from those by Heaslet and Warming near the boundary surfaces because the boundary conditions do not account for unattenuated radiative transfer from the opposite wall. In all cases, the P-1 approximation tends to underestimate the emissive power at the hot surface and overestimate the emissive power at the cold surface. Note, however, that the "exact" results are obtained when the optical thickness approaches the transparent limit ($\tau_0 = 0$).

The effects of varying the cold wall emissivity on the emissive powers of the medium at the cold wall are shown in Figure 4.3. The effects of varying the cold wall emissivity on the heat transfer are shown in Figure 4.4. As discussed earlier, the maximum deviation from the emissive power profile occurs at the walls. As the wall emissivity decreases or the optical thickness increases, the P-1 approximation emissive power profile approaches the exact solution. The same trend is found in Figure 4.4 where the heat transfer rate approaches the exact solution. Note that, as the cold wall emissivity decreases, the emissive powers approach that of the hot wall and the heat transfer rate approaches zero.

A more detailed comparison of the P-1 results and the analytical solution is presented in Tables 4.1 and 4.2. Table 4.1 summarizes heat transfer results for both walls having the same emissivity. Table 4.2 summarizes results for a wall one emissivity of unity and variable wall two emissivity. In all cases the P-1 approximation tends to overestimate the radiant heat transfer rate. The percent error was calculated using the expression:

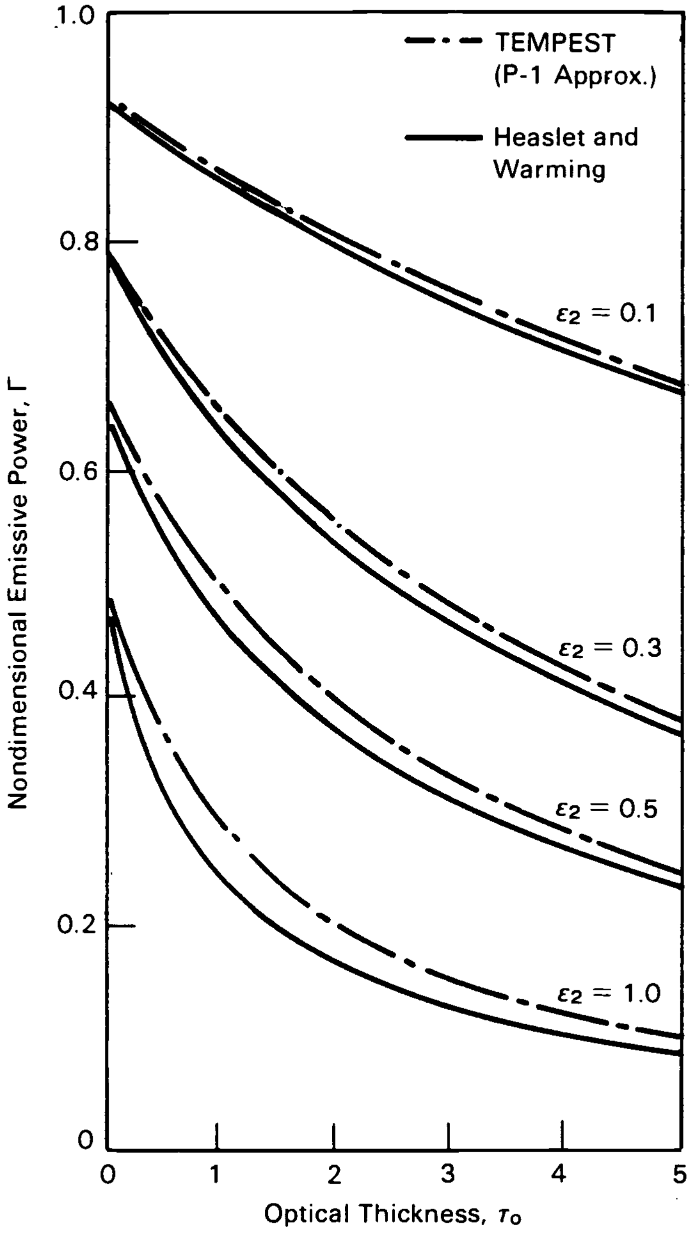

Figure 4.3. Nondimensional emissive powers at the cold wall for different wall two emissivities (ε_1 = 1.0)

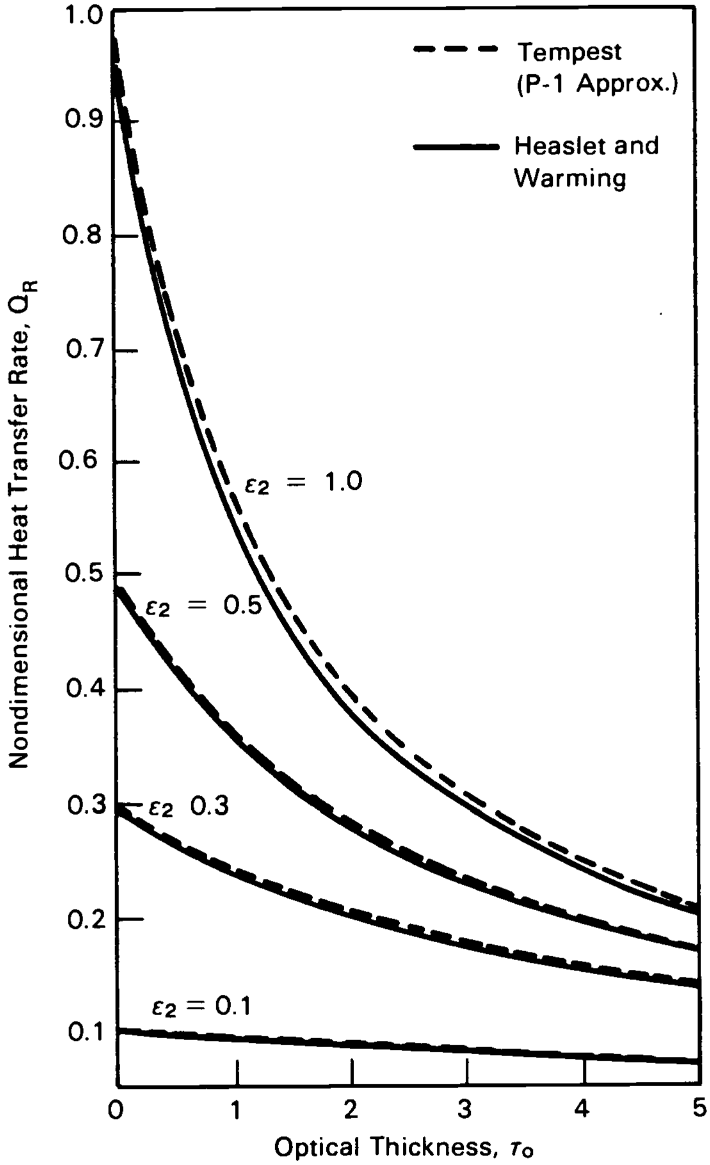

Figure 4.4. Nondimensional heat transfer rates between parallel plates for different wall two emissivities (ε_1 = 1.0)

Table 4.1. Nondimensional Heat Transfer for Walls Having the Same Emissivity ($\tau_0 = 1.0$, $\varepsilon_1 = \varepsilon_2$)

Wall Emissivity (ε)	P-1 Approx.	Analytical[(a)] Solution	% Error
1.0	0.5714	0.5532	3.29
0.5	0.2667	0.2626	1.56
0.1	0.0506	0.0505	0.20

Table 4.2. Nondimensional Heat Transfer for Different Wall Two Emissivities ($\tau_0 = 1.0$, $\varepsilon_1 = 1.0$)

Wall Two Emissivity (ε)	P-1 Approx.	Analytical[(a)] Solution	% Error
1.0	0.5714	0.5532	3.29
0.5	0.3636	0.3562	2.08
0.1	0.0930	0.0925	0.54

a) Reference Heaslet and Warming 1965.

$$|\%\ \text{Error}| = \left|\frac{X_{P-1} - X_{\text{reference}}}{X_{\text{reference}}}\right| \times 100\% \qquad (4.6)$$

The maximum error for the P-1 approximation was less than 4 percent. For the parallel plate geometry, the P-1 approximation and diffusion theory solutions are identical.

Another problem which is of interest is the evaluation of heat transfer between infinite concentric gray cylinders separated by a gray gas. A comparison of nondimensional heat transfer rates for the P-1 approximation, diffusion theory, and the Monte Carlo numerical solution is shown in Figure 4.5 as a function of optical thickness. The results are for black concentric cylinders with a two-to-one diameter ratio and the parameter Q_R is defined using the inside cylinder heat flux. In this case, a dramatic difference in heat transfer rates is evident, especially for small optical thicknesses. To understand the difference in the three methods, compare the expressions for nondimensional heat transfer in the case of $\tau_o = 0$. The expression for the exact solution (with $\tau_o = 0$) is

$$Q_R = \frac{1}{\frac{1}{\varepsilon_1} + \frac{D_1}{D_2}\left[\frac{1}{\varepsilon_2} - 1\right]} \qquad (4.7)$$

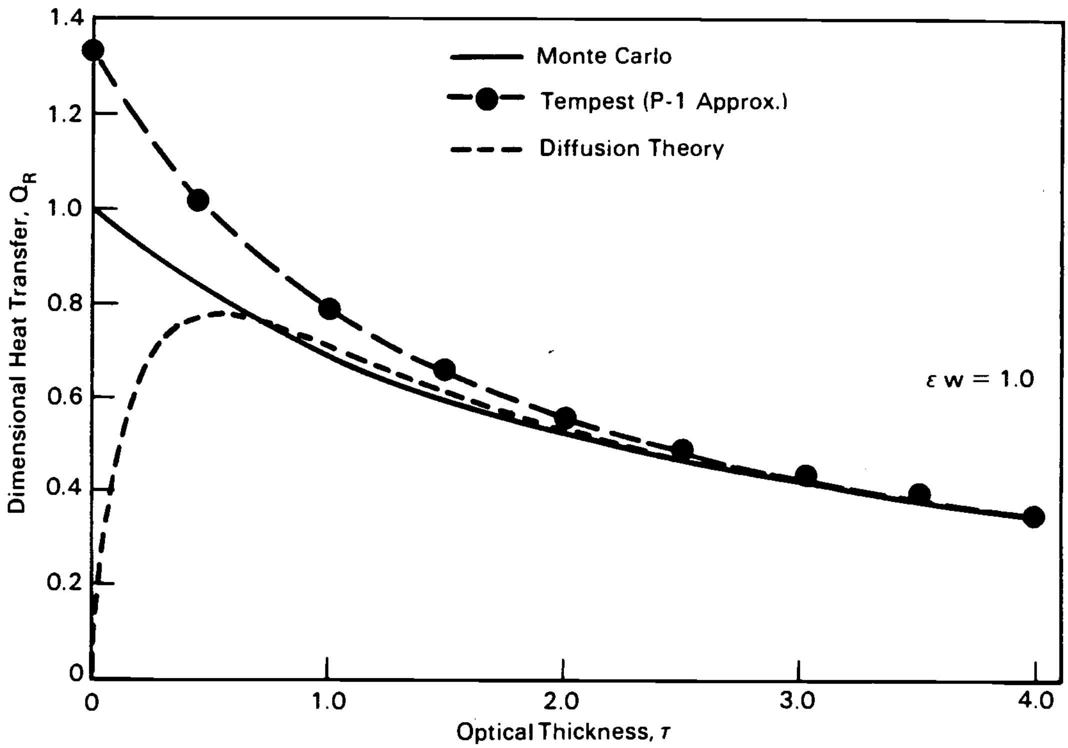

Figure 4.5. Comparison of heat transfer rates between concentric black cylinders ($D_{inner}/D_{outer} = 0.5$)

where ε_1 and ε_2 are the inside and outside wall emissivities, respectively. For the case of black cylinders, Q_R is unity. The expression resulting from diffusion theory using a second-order slip boundary condition is

$$Q_R = \frac{1}{\frac{3}{8}\left[\kappa\, D_1 \ln\left(\frac{D_2}{D_1}\right) + \frac{1-(D_1/D_2)^2}{\kappa\, D_1}\right] + \frac{1}{\varepsilon_1} - \frac{1}{2} + \frac{D_1}{D_2}\left[\frac{1}{\varepsilon_2} - \frac{1}{2}\right]} \qquad (4.8)$$

Note that, as κ approaches zero,the second term in the denominator drives the solution to zero. As a result, only when the optical thickness is very large does the diffusion theory method provide reliable results.

The expression for nondimensional heat transfer using the P-1 approximation for the case of $\tau_0 = 0$ is derived in Appendix B and takes the form

$$Q_R = \frac{1}{\frac{1}{\varepsilon_1} + \frac{D_1}{D_2}\left[\frac{1}{\varepsilon_2} - \frac{1}{2}\right] - \frac{1}{2} + \frac{3\kappa}{8} D_1 \ell n \frac{D_2}{D_1}} \tag{4.9}$$

$$= \frac{1}{\frac{1}{\varepsilon_1} + \frac{D_1}{D_2}\left[\frac{1}{\varepsilon_2} - 1\right] + E}$$

$$E = \frac{D_1}{2D_2} - \frac{1}{2} + \frac{3\kappa}{8} D_1 \ell n \frac{D_2}{D_1}$$

where E represents the terms in the denominator which do not match those of the exact solution. As κ approaches zero the third term in E disappears. It appears that the maximum error in the heat transfer rate is dependent on both the geometry and wall emissivities. This is more clearly seen in Figure 4.6, which shows the ratio of predicted to actual heat transfer rates at $\tau_0 = 0$ as a function of diameter ratio and wall emissivity. As the diameter ratio approaches unity, the cylindrical solution becomes that for parallel plates, which is exact at $\tau_0 = 0$. As the diameter ratio increases, the predicted heat transfer rate asymtotically approaches twice the actual rate. The limit is reduced as the wall emissivity decreases.

4.3.2 Two-Dimensional Geometry

The first case considered is a simple two-dimensional rectangular enclosure consisting of four isothermal black walls containing a gray participating gas. It is assumed that three of the walls have a temperature and emissive power of zero and the other wall (designated as wall one) has a higher temperature. It is important to note that temperature dicontinuities exist at the intersection of wall one with adjacent walls. At these corners the assumption that higher-order moments may be neglected is not valid. Therefore, this problem will be more severe than most practical problems where discontinuities do not exist.

The results presented for this problem are given in terms of nondimensional parameters. The optical thickness in the x_1 (perpendicular to wall one) is assumed to be unity. The optical thickness in the x_2 direction is dependent on the aspect ratio of

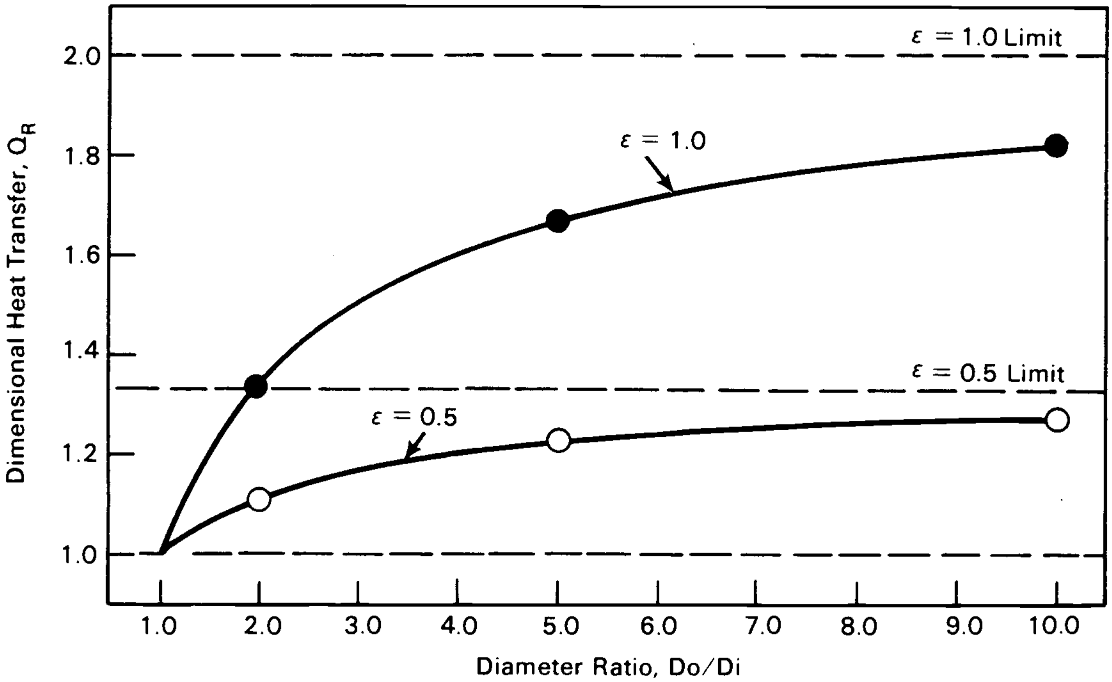

Figure 4.6. Ratios of predicted to actual heat transfer rates as a function of cylinder diameter ratios ($\varepsilon_1 = \varepsilon_2 = 1.0$, $\tau_o = 0$)

the rectangular enclosure. The variables n and x signify the optical distance in the x_1 and the x_2 directions, respectively. The nondimensional emissive power is represented by the parameter B, which is defined as

$$B(x,n) = \frac{e_b\ (x,n)}{e_{b1}} \tag{4.10}$$

where e_{b1} is the black body emissive power of wall one.

The P-1 results are compared with those obtained by Modest (1975) using the differential approximation and correcting for moderately thick and optically thin medium by introducing a number of geometrical parameters. The governing energy and emissive power equations with the included correction factors reduce to the exact solution for the optically thin and thick limits with good accuracy for all intermediate optical thicknesses. This approach was verified by comparison with detailed numerical solutions using Hottel's zone method.

The centerline emissive power profiles resulting from the P-1 solution method are compared with those from Modest in Figure 4.7 for different aspect ratios. The comparison of emissive powers at the walls is not as good as in the one-dimensional case. This is partly due to the temperature discontinuity at the corners. Since the walls are black, the hot wall infinitesimally near the corner is emitting and absorbing and the cool walls infinitesimally near the corner are only absorbing. Neglecting the higher moment terms essentially assumes that they are zero. This reduces the resistance to radiant energy transfer and results in a higher heat transfer rate and more moderate emissive powers at the walls. Therefore, the P-1 results underestimate the emissive power near the hot surface and overestimate the emissive power near the cool surface. Note that as the aspect ratio (r) increases, the effect of the corners become less important and the solution approaches that of the one-dimensional case for an optical thickness of one.

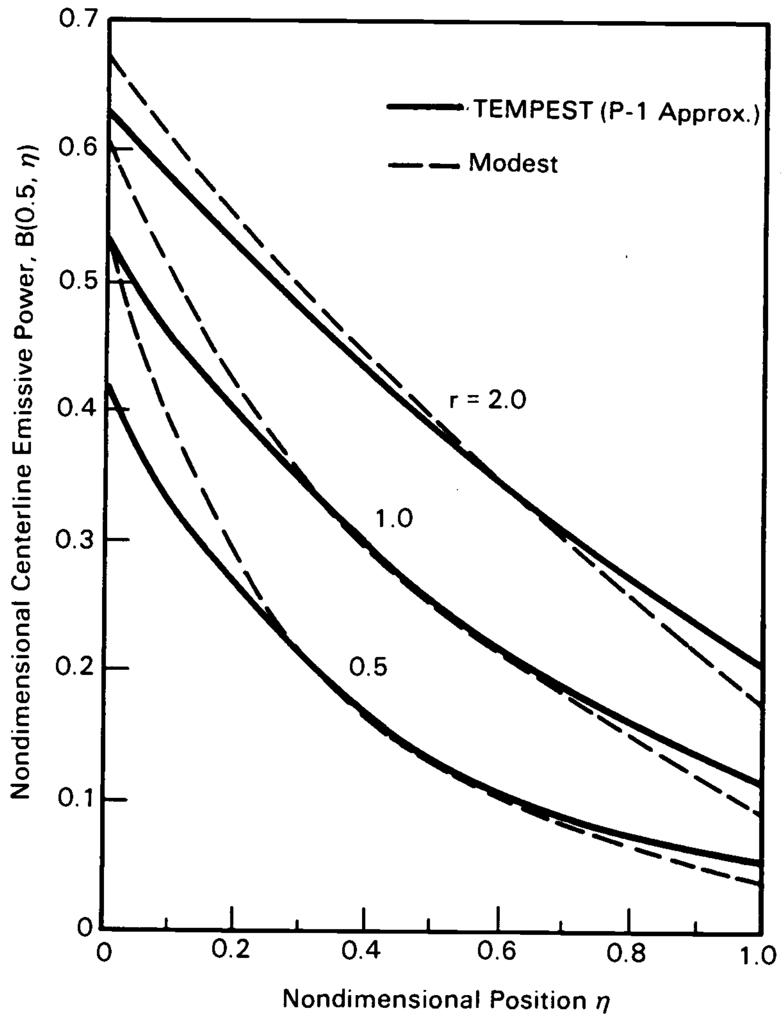

Figure 4.7 Comparative Nondimensional Centerline Emissive Power Distributions for Different Aspect Ratios: $\tau_1 = 1.0$, $B_1 = 1.0$, $B_i = 0.0$ ($i = 2\text{-}4$), $\varepsilon_i = 1.0$ ($i = 1\text{-}4$)

The effect of varying the hot wall emissivity in a square enclosure with an optical thickness of unity in both directions is shown in Figure 4.8. The cool walls are blackbody surfaces and the hot wall surface emissivity is varied between $\varepsilon_1 = 1.0$ and $\varepsilon_1 = 0.1$. Note that, as in the one-dimensional case, the comparison of results improve as the emissivity decreases.

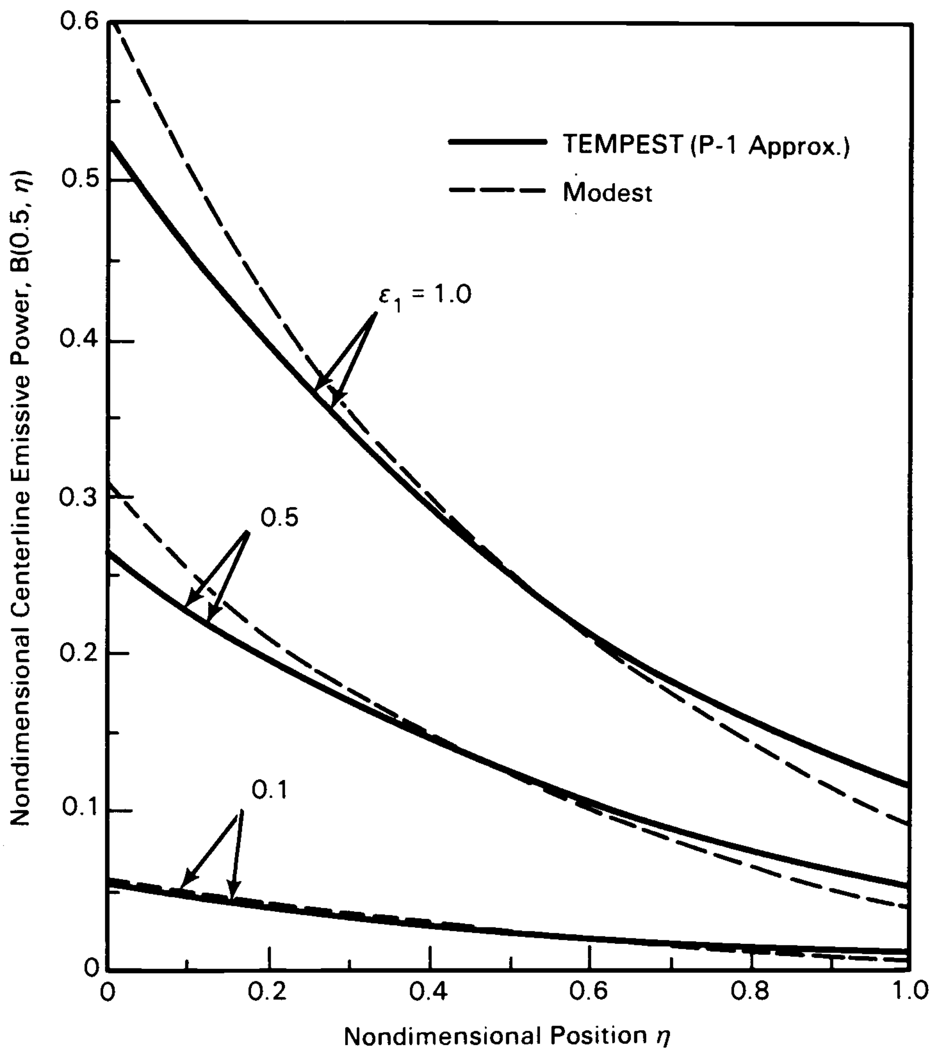

Figure 4.8 Comparative Nondimensional Centerline Emissive Power Distributions in a Square Enclosure for Different Wall One Emissivities: $\tau_1 = \tau_2 = 1.0$, $r = 1.0$, $B_1 = 1.0$, $B_i = 0.0$ ($i = 2$-4), $\varepsilon_i = 1.0$, ($i = 2$-4)

5.0 EVALUATION: RADIATION AND CONDUCTION

5.1 INTRODUCTON

In the previous chapter the results of the P-1 radiation model for purely radiant heat transfer problems was evaluated using existing analytical and numerical solutions. However, for most practical problems the heat transfer through a participating medium will be affected by both conduction and radiation heat transfer. In this case, thermal radiative equilibrium does not exist and energy is passed between the radiative transfer solution and the thermal energy solution. To evaluate the interaction of the two solution procedures, the results for combined radiation-conduction problems will be compared with existing analytical solutions.

5.2 REVIEW OF LITERATURE

A significant amount of literature exists for one-dimensional radiation-conduction problems. The simplest problem which may be considered is the calculation of heat transfer and temperature distribution between infinite parallel gray plates of different temperatures separated by a conducting and participating medium. The earliest "exact" solutions to this problem were performed by Viskanta (1965) and Viskanta and Grosh (1962) using a numerical iterative solution of the governing nonlinear integral equation. Later, Crosbie and Viskanta (1971) expanded the Viskanta work to include nongray medium effects. More recently, Yuen and Wong (1980) have extended the successive approximation method for use in radiation-conduction problems. They have shown good agreement with work reported by Viskanta and Crosbie for the higher approximation solutions.

To date, there has been little work in the area of two-dimensional problems involving combined radiation-conduction. Most work has incorporated either the optically thin or thick approximations. One notable exception is the work done by Ratzel (1981), who used the P-1 and P-3 approximations to obtain solutions for a square enclosure. However, no exact solution has been found in the literature.

To characterize a heat transfer problem where both radiation and conduction are involved, the relative importance of the two heat transfer modes must be specified. This is done using the conduction-radiation parameter, also known as the Stark number, which is defined as

$$N_j = \frac{ka}{4\sigma T_j^3} \qquad (5.1)$$

based on the jth temperature. This dimensionless parameter is an approximate ratio of the heat transfer rate by conduction to that by radiation. For $N = \infty$, heat transfer within the medium is only by conduction. The opposite extreme of N=0 corresponds to the case in which heat transfer is solely due to radiation. For most gases of practial engineering interest, the value for N falls in the region of 0.01-0.1, which indicates a radiation dominant problem. For example, values of N (based on the Planck mean absorption coefficient) are illustrated in Figure 5.1 for ammonia, carbon dioxide and water vapor.

5.3 EVALUATION OF RESULTS

The first case considered is the calculation of heat transfer and temperature disbribution between infinite parallel gray plates at different temperatures separated by a conducting and participating medium. Dimensionless temperatures will be represented by the parameter, Θ, which is defined as

$$\Theta\ (\tau) = \frac{T(\tau)}{T_1} \tag{5.2}$$

where τ is the optical depth from the hot wall and T_1 is the peak wall temperature. The heat transfer rate is represented by the dimensionless parameter, Q_T, which is defined as

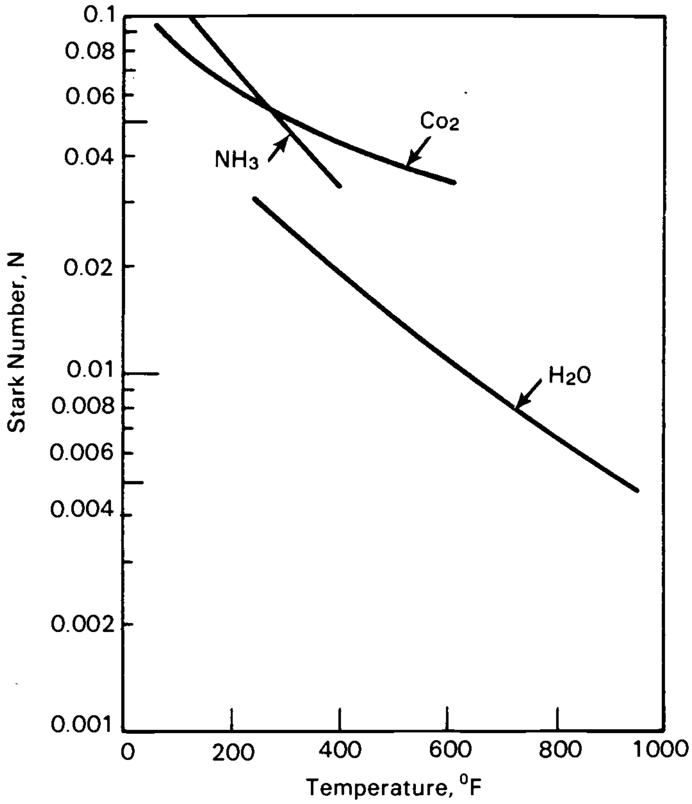

Figure 5.1. Values for the Stark number, N, for Ammonia, Carbon Dioxide and Water at One Atmosphere

$$Q_T(\tau) = \frac{q_R(\tau) + q_c(\tau)}{e_{b1}} \tag{5.3}$$

where q_R and q_c are the radiation and conduction heat transfer rates and e_{b1} is the emmissive power of the hot wall.

Figures 5.2 and 5.3 show the effects of decreasing Stark number on the temperature distribution in a medium in which the optical thickness is moderate (τ_0 = 1.0) and the absolute wall temperature ratios are H = 0.1 and 0.5. The limiting radiation solution N_1 = 0 is from Heaslet and Warming (1965), as described in Chapter 4, and the result for $N_1 = \infty$ is the one-dimensional conduction solution. The P-1 results for intermediate values for N are compared with those obtained by Viskanta and Grosh (1962). Note that, when the Stark number decreases, the temperature distribution attempts to approach the radiative solution in the interior of the medium. However, since conduction is involved, there can be no "slip" at the walls, as there was for the radiant heat transfer results presented in Chapter 4, and the medium temperature must approach that of the walls in the vicinity of the wall.

A more detailed comparison of the P-1 results and analytical solutions is presented in Tables 5.1 and 5.2. Table 5.1 summarizes heat transfer results for the three optical thicknesses (τ_0 = 0.1, 1.0, 10.0) with the Stark numbers ranging from strongly radiation-dominated to conduction-dominated. As in the radiative transfer studies, the P-1 approximation tends to overestimate the total heat transfer for the cases considered. The percent error was calculated using the expression:

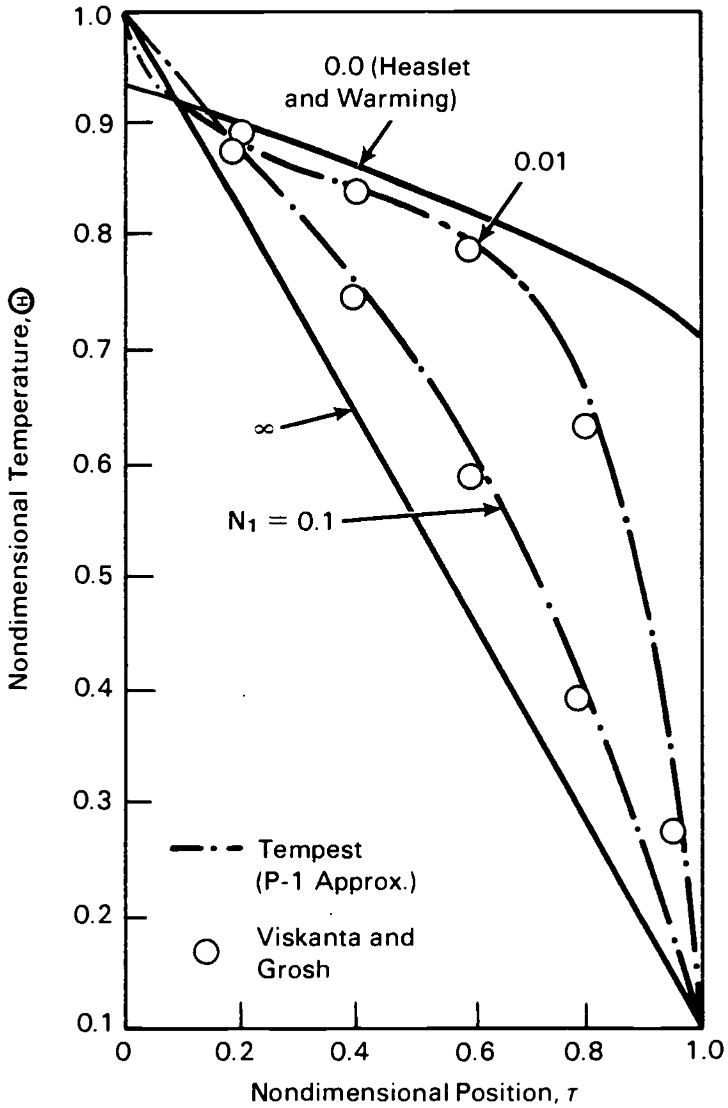

Figure 5.2. Nondimensional Temperature Profiles Between Parallel Plates for Different Stark Numbers: (τ_0 = 1.0, $\varepsilon_1 = \varepsilon_2$ = 1.0, Θ = 0.1)

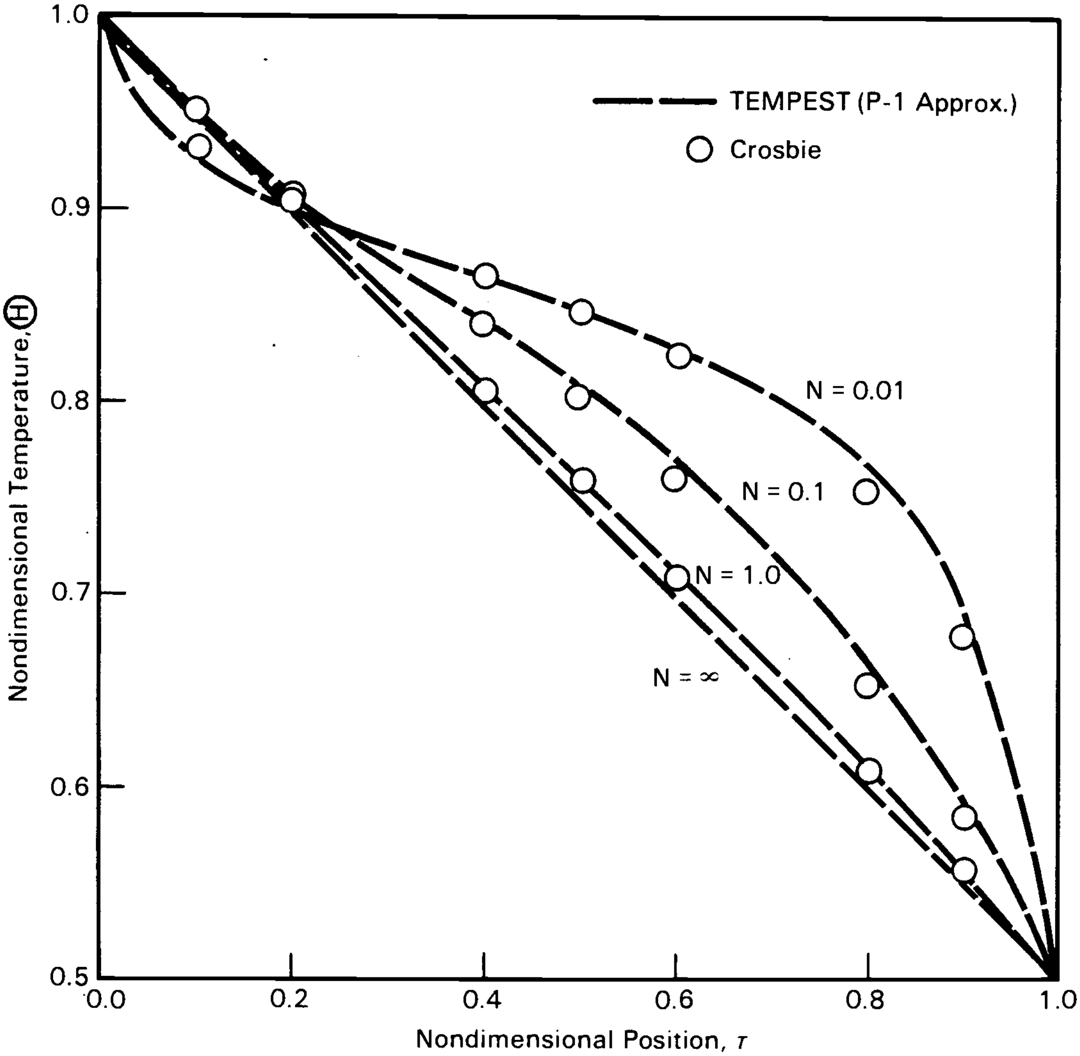

Figure 5.3. Nondimensional Temperature Profiles Between Parallel Plates for Different Stark Numbers: (τ_o = 1.0, ε_1 = ε_2 = 1.0, Θ = 0.5]

Table 5.1. Nondimensional Heat Transfer Comparison ($\varepsilon_1 = \varepsilon_2 = 1.0$, $\Theta = 0.5$)

Optical Thickness (τ_0)	Stark Number (N)	P-1 Approx.	Analytical Solution[a]	% Error
	0.0		0.8585	
	0.01	1.097	1.080	1.57
0.1	0.1	2.898	2.880	0.63
	1.0	20.90	20.88	0.10
	10.0	200.97	200.88	0.04
	0.0		0.5188	
	0.01	0.5934	0.5675	4.56
1.0	0.1	0.8079	0.7694	5.00
	1.0	2.614	2.572	1.63
	10.0	20.62	20.57	0.24
	0.0		0.1095	
	0.01	0.1140	0.1131	0.80
10.0	0.1	0.1344	0.1335	0.67
	1.0	0.3164	0.3150	0.44
	10.0	2.117	2.115	0.09

a) Reference Crosbie and Viskanta 1971.

Table 5.2. Nondimensional Temperature Distribution Comparison ($\tau_0 = 1.0$, $\varepsilon_1 = \varepsilon_2 = 1.0$, $\Theta = 0.5$)

Stark Number (N_1)	Optical Depth (τ)	P-1 Approx.	Analytical Solution[a]	% Error
	0.0	1.0000	1.0000	0.00
	0.1	0.9234	0.9313	0.85
	0.2	0.8986	0.9046	0.66
	0.4	0.8640	0.8657	0.20
0.01	0.5	0.8461	0.8456	0.06
	0.6	0.8265	0.8232	0.40
	0.8	0.7678	0.7548	1.72
	0.9	0.6939	0.6762	2.62
	1.0	0.5000	0.5000	0.00
	0.0	1.0000	1.0000	0.00
	0.1	0.9472	0.9504	0.34
	0.2	0.9085	0.9105	0.22
	0.4	0.8429	0.8407	0.26
0.1	0.5	0.8085	0.8032	0.66
	0.6	0.7691	0.7611	1.05
	0.8	0.6636	0.6538	1.50
	0.9	0.5910	0.5838	1.23
	1.0	0.5000	0.5000	0.00
	0.0	1.000	1.000	0.00
	0.1	0.9504	0.9508	0.04
	0.2	0.9027	0.9027	0.00
	0.4	0.8084	0.8073	0.14
1.0	0.5	0.7605	0.7588	0.22
	0.6	0.7115	0.7095	0.28
	0.8	0.6092	0.6074	0.30
	0.9	0.5556	0.5544	0.22
	1.0	0.5000	0.5000	0.00

a) Referenced in Ratzel 1981.

$$|\%\ \text{Error}| = \left|\frac{X_{P-1} - X_{reference}}{X_{reference}}\right| \times 100\% \qquad (5.4)$$

The maximum errors for the P-1 approximation rarely exceeded 5 percent in predicting the heat transfer rates.

Table 5.2 presents temperature distributions in a moderate optical thickness medium (τ_0 = 1.0) for three Stark numbers (N_1 = 1.0, 0.1, 0.01). The exact results were obtained from Crosbie, as reported in Ratzel (1981), and are from work which he completed with Viskanta. As in the case of pure radiant heat transfer, the P-1 approximation tends to underpredict the temperature near the hot surface and overpredict near the cool surface. The errors were calculated at selected points in the profile and the maximum error rarely exceeded 2 percent in predicting the temperature distribution.

In addition to solutions for problems with black walls, analytaical solutions have been obtained for walls with various emissivities. Table 5.3 shows a comparison of heat transfer results for wall emissivities of 1.0, 0.5, and 0.1. As the emissivity is reduced, the amount of reduction in the heat transfer is strongly dependent on the Stark number. The errors are similar to those obtained for the black wall case. Temperature distributions are not presented since, with the no-slip boundary conditions, the temperature profiles are similar to

Table 5.3. Nondimensional Heat Transfer Comparison for Different Wall Emissivities (τ_0 = 1.0, Θ = 0.5)

Optical Emissivity ($\varepsilon_1=\varepsilon_2$)	Stark Number (N)	P-1 Approx.	Analytical Solution[a]	% Error
	1.0	2.614	2.572	1.63
1.0	0.1	0.8079	0.769	5.00
	0.01	0.5934	0.567	4.56
	0.0		0.5186	
	1.0	2.400	2.364	1.52
0.5	0.1	0.5816	0.5704	1.96
	0.01	0.3393	-	-
	0.0		0.2462	
	1.0	2.259	2.221	1.71
0.1	0.1	0.4284	0.403	6.30
	0.01	0.1625	0.158	2.85
	0.0		0.0474	

(a) Reference Yuen and Wong 1980.

those presented in Table 5.2 and Figures 5.2 and 5.3 for the black case.

For all previous results presented it has been assumed that the extinction coefficient, κ, consisted entirely of the absorption coefficient, a. Recall that the scattering albedo, Ω_0, is defined as

$$\Omega_0 = \frac{\sigma_s}{a+\sigma_s} = \frac{\sigma_s}{\kappa} \tag{2.8}$$

where σ_s is the scattering coefficient. For $\Omega_0 = 0.0$, which corresponds to the results presented so far, the radiative resistance is due solely to absorption by the medium.
For $\Omega_0 = 1.0$, there is no absorption and the radiant and thermal solutions are totally independent of each other. The nondimensional temperature profiles for varying scattering albedo are shown in Figure 5.4. The temperature profile is independent of the Stark number for $\Omega_0 = 1.0$ and is in fact identical to the conduction solution.

The effect of the scattering albedo on the combined heat transfer is shown in Table 5.4. In all cases, the heat transfer decreases with increasing scattering albedo, which indicates that the conduction and radiation modes of heat transfer are more efficient at removing heat when they interact with each other. The value for the scattering albedo becomes more significant as the Stark number decreases. The P-1 approximation tends to overestimate the heat transfer, but the maximum error is less than four percent.

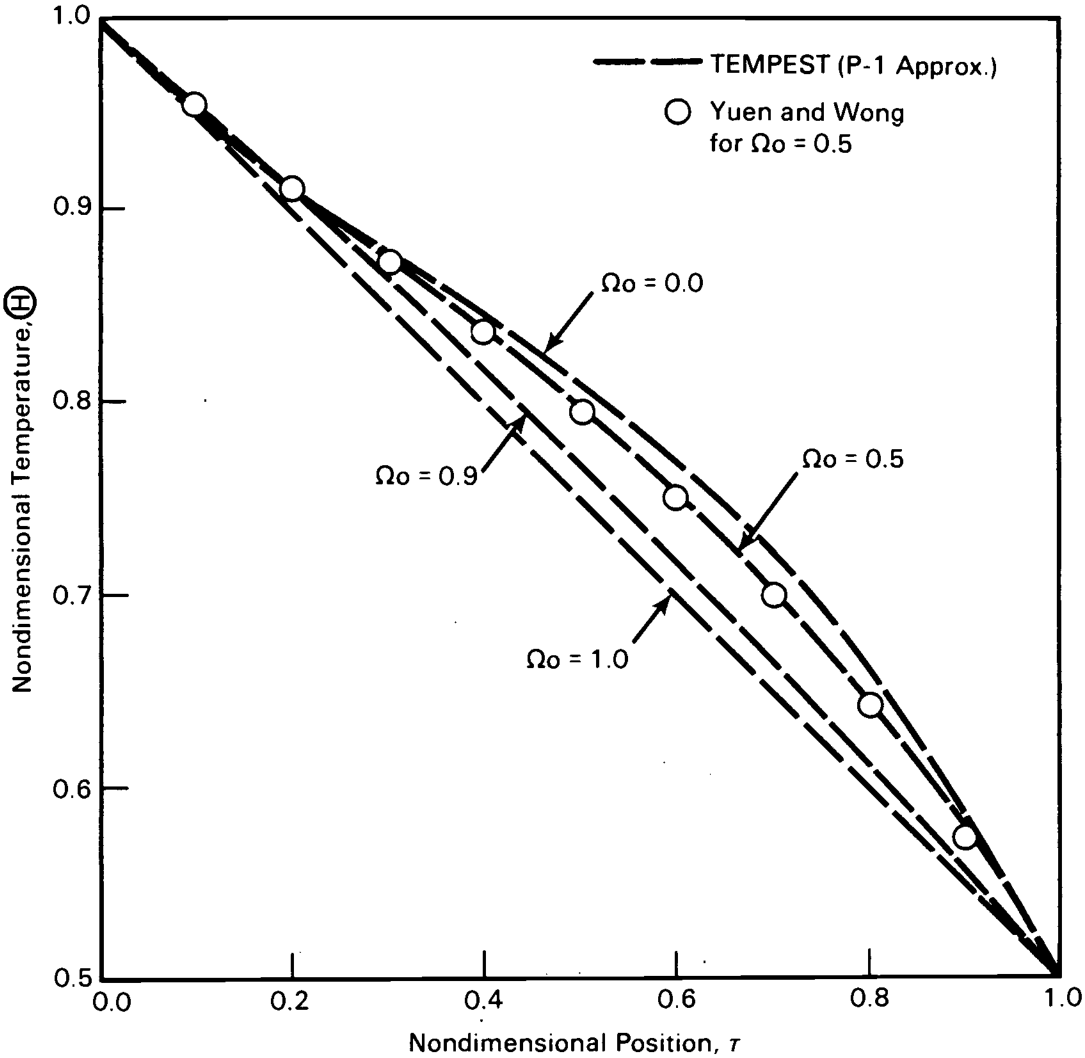

Figure 5.4. Nondimensional Temperature Profiles for Different Scattering Albedos: (τ_o = 1.0, $\varepsilon_1 = \varepsilon_2$ = 1.0, N_1 = 0.1, Θ = 0.5)

Table 5.4. Nondimensional Heat Transfer Comparison for Different Scattering Albedo ($\varepsilon_1 = \varepsilon_2 = 0.1$, $\Theta = 0.5$)

Optical Thickness (τ)	Stark Number (N_1)	P-1 Approx.	Analytical Solution[a]	% Error
	0.0	0.163	0.158	3.16
0.01	0.5	0.133	0.130	2.31
	1.0	0.067	0.067	0.00
	0.0	0.428	0.403	6.20
0.1	0.5	0.357	0.346	3.18
	1.0	0.248	0.247	0.40
	0.0	2.259	2.221	1.71
1.0	0.5	2.167	2.154	0.60
	1.0	2.048	2.047	0.05
	0.0	0.307	0.305	0.66
1.0	0.5	0.301	0.299	0.66
	1.0	0.235	0.235	0.00
	0.0	2.108	2.106	0.09
10.0	0.5	2.103	2.101	0.09
	1.0	2.035	2.035	0.00
	0.0	20.109	20.105	0.02
100.0	0.5	20.104	20.100	0.02
	1.0	20.035	20.035	0.00

(a) Referenced in Yuen and Wong 1980.

6.0 EVALUATION: RADIATION, CONDUCTION, AND CONVECTION

6.1 INTRODUCTION

In previous chapters the results of the P-1 radiation model were evaluated for problems involving only radiation heat transfer or both radiation and conduction. There are many problems where participating media radiation and conduction are the only modes of heat transfer. A good example of this is heat transfer through solid glass. However, in most practical problems where the medium absorbs, emits, and scatters radiation, the medium is generally in the form of a gas. Therefore, convection is potentially an important mode of heat transfer. To evalute the effect of convection on the thermal energy solution, the results for problems involving all three modes of heat transfer will be compared with existing analytical solutions.

6.2 REVIEW OF LITERATURE

A limited amount of literature exists for one-dimensional problems involving radiation, conduction, and convection. The simplest problem which may be considered is the calculation of heat transfer and temperature distribution between infinite parallel gray plates separated by a steady flow of conducting and participating medium. Various velocity profiles were considered. Solutions for slug flow velocity profile were obtained by Viskanta (1964) and Chen (1964) by expanding the emissive power in a Taylor series and solving the resulting equations. Similar solutions were obtained for Couette flow by Viskanta and Grosh (1961) and later by Viskanta (1965). One of the most complete analyses of flow between plates was performed by Viskanta (1965) for a parabolic velocity profile which is representative of fully developed laminar flow. In this analysis it is assumed that both plates are the same temperature, and the fluid enters at a significantly higher or lower temperature. The resulting temperature profiles are obtained as a function of the Stark number, N, and the dimensionless fluid centerline temperature. The results of this analysis will be used for comparison.

Very little work has been done in the area of two-dimensional radiation, conduction, and convection heat transfer. Two analyses have been presented by Einstein for slug flow through parallel-plate (Einstein 1963) and circular tube (Einstein 1963) channels of finite length. However, in both studies the integrodifferential energy equation was replaced by a system of algebraic equations using Hottels zonal method and are not sufficiently accurate to use for comparison.

6.3 EVALUATION OF RESULTS

The case being considered is the calculation of temperature distribution between infinite parallel gray plates separated by a steady flow of conducting and participating medium. In this analysis it is assumed that both plates are the same temperature and the fluid enters at significantly higher or lower temperature. The temperatures will be represented by the dimensionless parameter, Θ, which is defined as

$$\Theta(\tau) = \frac{T(\tau)}{T_w} \tag{6.1}$$

where τ is the optical depth from either wall and T_w is the wall temperature.

This analysis is one-dimensional and it is assumed that fully-developed temperature profile is established. The condition used by Viskanta to define this profile is an expression given by Seban and Shimazaki (1951) for fully developed flow at distances far away from the entrance to describe the axial temperature gradient

$$\frac{\partial T}{\partial x} = \left(\frac{T_w - T}{T_w - T_m}\right) \frac{dT_m}{dx} \tag{6.2}$$

where T_m is the mixing cup temperature. This expression simply states that the axial temperature gradient at any point is directly proportional to the temperature difference between that point and the wall. However, this expression was developed for situations involving only conduction and convection. Since radiation is highly nonlinear in temperature, this expression would only be valid where the contribution of radiation is very small. Therefore, to provide a direct comparison between TEMPEST results and the analytical solution, the inlet temperature profile was artificially adjusted until the condition specified in Equation 6.2 was satisfied.

Figure 6.1 shows the effect of decreasing Stark number on the temperature distribution in the medium for a moderate optical thickness ($\tau_o = 1.0$) and a dimensionless centerline temperature of $\Theta = 0.5$. Since the channel has half symmetry, only half of the profile is shown. The exact temperature profiles for the case when energy is transported only by conduction and convection ($n = \infty$) and the computed profile for convection and radiation ($N = o$) are included for comparison. As N decreases, the temperature field departs more and more from that of pure conduction and convection.

Note that the P-1 results tend to deviate from the analytical solution for lower values of N. This is especially noticeable near the wall. One reason for this is the boundary conditions used in the two methods. The boundary condition used by Viskanta is defined by the expression

$$B(o) = B(\tau_0) = \frac{\varepsilon H_w^4 + 2(1-\varepsilon) \int_0^{\tau_0} \Theta^4(\tau)\, E_2(\tau) d\tau}{1 - 2(1-\varepsilon)\, E_3(\tau_0)} \qquad (6.3)$$

$$E_n(\tau) = \int_0^1 \mu^{n-2} \exp(-\tau/\mu) d\mu$$

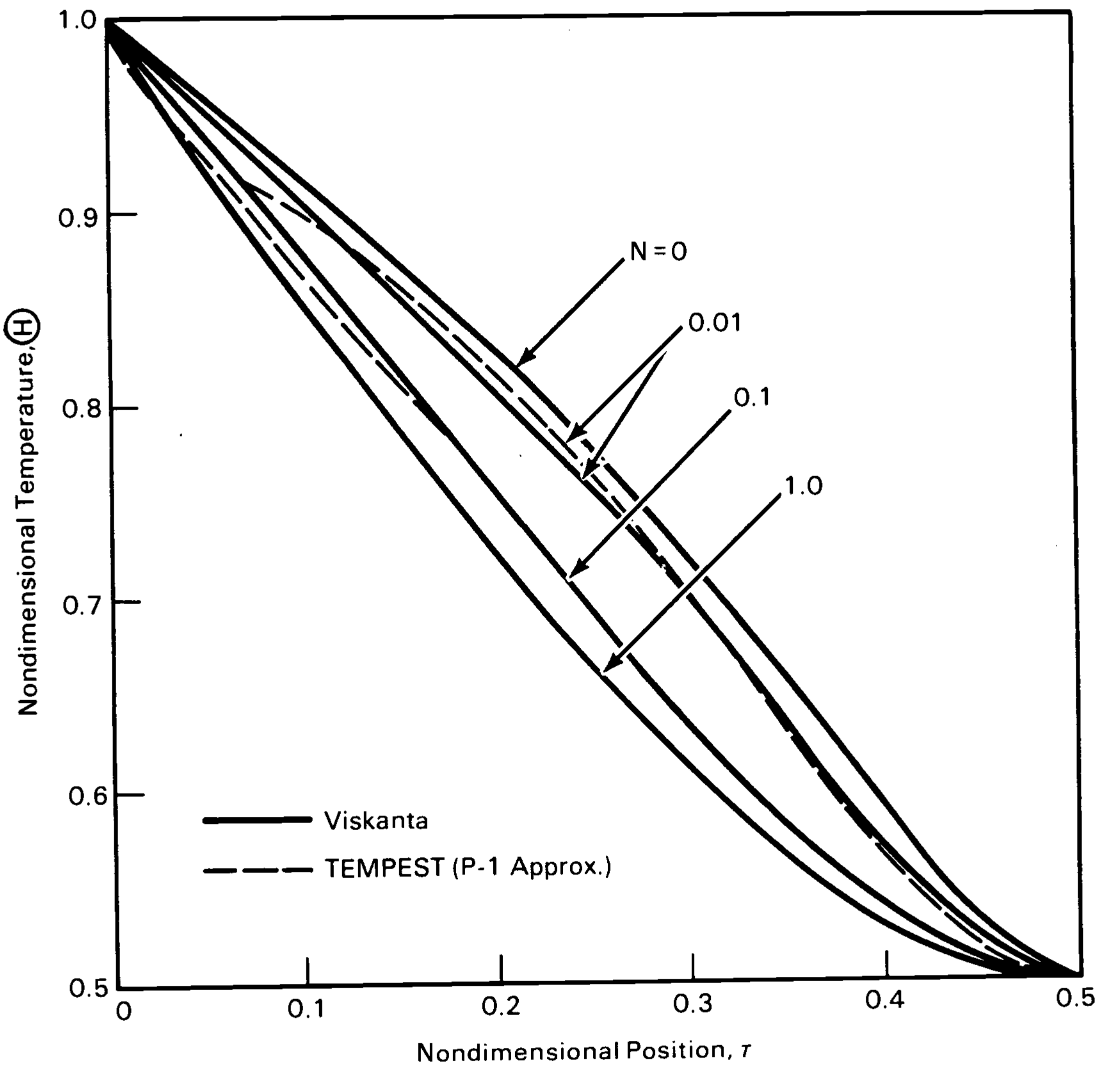

Figure 6.1 Nondimensional Temperature Profiles of Flow Between Parallel Plates for Different Stark Numbers: $\tau_o = 1.0$, $\varepsilon_1 = \varepsilon_2 = 1.0$)

where B is the dimensionless radiosity and ε is the emissivity of the wall. For the situation where $\varepsilon = 1$, the radiosity at the wall simply becomes the emissive power of the wall. This is evident in the convection and radiation (N=0) temperature profile. As discussed in the previous two chapters, when there is no conduction and a small or moderate optical thickness, a temperature slip should exist at the boundary. The reason given by Viskanta for this discrepancy is that only the first three terms of the Taylor series expansion of $\Theta^4(\tau)$ were used in deriving the equations. In comparison, the P-1 results show a sharper drop near the wall indicating the effect of the "slip" condition at the wall. Therefore, an improved comparison could be expected when consistent boundary conditions are used.

7.0 CONCLUSIONS AND RECOMMENDATIONS

7.1 SUMMARY

In this work, a method for solving the differential form of the radiative transfer equation was implemented into an existing three-dimensional thermal-hydraulic computer program known as TEMPEST. The method used was the P-1 approximation, where the angular distribution of the radiation intensity is represented by a truncated series of spherical harmonics. When this series is substituted into the radiant energy transfer equation, and closure conditions are applied, a single second-order partial differential equation results. The appropriate Marshak boundary conditions were also developed.

Once the P-1 formulation had been developed, it was implemented in the TEMPEST computer program. The governing partial differential equation was cast in a three-dimensional finite-difference form. The equation is solved using the line successive overrelaxation (LSOR) method with occasional rebalancing to enhance convergence. The existing energy equations in TEMPEST were also modified to account for the thermal energy emitted or absorbed in each cell due to thermal radiation.

To determine the accuracy and limits of the P-1 formulation, a series of comparisons were made between TEMPEST results and existing solutions. Evaluations were made for problems involving thermal radiation only, radiation and conduction, and finally, radiation, conduction, and convection.

In the pure radiation case, comparison of results were made for three different geometries. The P-1 results for heat transfer and emissive power distribution between infinite parallel gray plates was compared with the exact formulation of Heaslet and Warming (1965) for different optical thicknesses. For large optical thicknesses ($\tau_0 > 1.0$), there was good agreement between differential and exact results. As the optical thickness decreased ($\tau_0 < 1.0$) the P-1 results deviated from the exact solution with the exception of an optical thickness of zero, where the P-1 solution is exact. When the surface emissivities of the walls were lowered, the agreement between the P-1 and exact results is improved. The maximum heat transfer error for an optical thickness of one was less than four percent.

The second problem considered was the calculation of heat transfer between infinite concentric gray cylinders. The P-1 results were compared with a Monte Carlo numerical solution by Perlmutter and Howell (1964). As in the parallel plate case, the comparison between the P-1 and Monte Carlo results improved as the optical thickness increased and the surface emissivity decreased. The heat transfer rate comparison was also highly dependent on the diameter ratio, ranging from no error for a diameter ratio (D_o/D_i) approaching one (parallel plate solution) to a factor of two overprediction for a diameter ratio approaching infinity and zero optical thickness. The results were acceptable for large optical thicknesses ($\tau_0 > 1.0$).

A simple two-dimensional rectangular enclosure consisting of four isothermal walls was evaluated for different aspect ratios. The centerline emissive power distributions resulting from the P-1 method were compared with those obtained by Modest (1975) using a modified differential method. The comparisons of results were acceptable for higher optical thicknesses but were not as good as in the parallel plate problem, due partly to the temperature discontinuity at the corners. As the aspect ratio increased, the results approached those of the parallel plate solution.

For the case of combined radiation and conduction heat transfer, both the P-1 method and the interaction with the TEMPEST thermal energy solution were evaluated. The P-1 results for heat transfer and temperature distributions between infinite parallel gray plates was compared with those obtained by Viskanta and Grosh (1962) using a numerical solution of the governing nonlinear integral equation. There was good agreement between results for optical thicknesses ranging from 0.1 to 10.0 and Stark numbers ranging from 0.01 to 1.0. The maximum deviation of the heat transfer rates rarely exceeded five percent and the temperature profiles differed by less than three percent in all cases. The best comparisons were obtained at the highest Stark numbers and optical thicknesses. A study of the effect of the scattering albedo indicated a decrease in total heat transfer with increasing scattering albedo.

The case of combined radiation, conduction, and convection was evaluated using the problem of parabolic flow between infinite parallel gray plates. The temperature distributions resulting from the P-1 method were compared with those obtained by Viskanta (1963) using a Taylor series approximation of the emissive power. Good agreement was obtained for larger Stark number values but the temperatures near the wall deviated as conduction decreased. This was due to the Taylor series approximation used in the boundary condition by Viskanta.

In general, the P-1 method yielded acceptable results for radiation problems with large optical thicknesses ($\tau_0 > 1.0$) or combined radiation and conduction problems with participating media. The accuracy of results for radiation problems involving little or no optical thickness are highly dependent on the geometry of the problem.

7.2 RECOMMENDATIONS

The P-1 approximation to the radiant energy transfer equation was selected to minimize the computational effort required to obtain a solution. However, if accuracy for problems involving small optical thicknesses is a major consideration, the P-3 approximation should be used. A significant improvement in accuracy has been demonstrated by Bayazitoglu and Higenyi (1979) for one-dimensional problems and Ratzel (1981) for two-dimensional problems. No attempt to extend the P-3 approximation to three-dimensions has been found. The resulting P-3 numerical method would involve solving four coupled second-order differential equations as opposed to one second-order differential equation for the P-1 method. It would be valuable if both the P-1 and P-3 methods would be included as options in TEMPEST with the P-3 method being selected only in the case of small optical thicknesses.

Another approximation which was made to simplify the analysis was the assumption that the medium was gray. In reality, the radiative properties of the medium are generally dependent on wavelength. A more accurate approximation would be to use medium energy band models and solve the P-1 equation for each energy band. The modification would result in a large increase in computational effort. An alternate approach would be to examine ways to better represent the radiative properties of the medium, such as $a(\lambda)$.

A major limitation of utilizing the P-1 method in the TEMPEST computer code is that the model is explicitly tied to the thermal energy equation. This could potentially limit the time step of certain problems where radiation is an important mode of heat transfer. A time step limit should be defined in terms of the thermal and geometrical problem parameters.

8.0 BIBLIOGRAPHY

Ames, W. F., 1977. Numerical Methods for Partial Differential Equations, Academic Press, New York.

Bayazitoglu, Y. and J. Higenyi, 1979. "Higher Order Differential Equations of Radiative Transfer: P_3 Approximation", AIAA Journal, Vol. 17, No. 4, pp. 424-431.

Chandrasekhar, S., 1960. Radiative Transfer, Dover Publications, Inc., New York.

Chen, C. 1964. "Simultaneous Radiative and Convective Heat Transfer in an Absorbing, Emitting, and Scattering Medium in Slug Flow Between Parallel Plates", AIChE Journal, Vol. 10, pp. 253-259.

Crosbie, A. L. and R. Viskanta, 1971. "Interaction of Heat Transfer by Conduction and Radiation in a Nongray Planar Medium", Warme und Stoffubertragung, Vol. 4, pp. 205-212.

Davison, B., 1958. Neutron Transport Theory, Clarendon Press, Oxford.

Deissler, R. G., 1964. "Diffusion Approximation for Thermal Radiation in Gases with Jump Boundary Conditions", J. Heat Transfer, C 86, pp. 240-246.

Douglas, J. Jr., and J. E. Gunn, 1964. "A General Formulation of Alternating Direction Methods", Numerical Mathematics, Vol. 6, p. 428.

Einstein, T. A., 1963. Radiant Heat Transfer to Absorbing Gases Enclosed between Parallel Flat Plates with Flow and Conduction, NASA Technical Report TR-R154.

Einstein, T. A., 1963. Radiant Heat Transfer to Absorbing Gases Enclosed in a Circular Pipe with Conduction, Gas Flow and Internal Heat Generation, NASA Technical Report TR-R156.

Eyler, L. L., D. S. Trent and M. J. Budden, 1983. TEMPEST - A Three-Dimensional Time-Dependent Computer Program for Hydrothermal Analysis, Volume II: Assessment and Verification Results, Technical Report PNL-4348, Vol. II, Battelle, Pacific Northwest Laboratory, Richland, Washington.

Glatt, L. and D. B. Olfe, 1973. "Radiative Equilibrium of a Gray Medium in a Rectangular Enclosure", J. Quantitative Spectroscopy and Radiative Transfer, Vol. 13, No. 9, pp. 881-895.

Heaslet, M. A. and R. F. Warming, 1965. "Radiative Transport and Wall Temperature Slip in an Absorbing Planar Medium", Int. J. Heat Mass Transfer, Vol. 8, No. 7, pp. 979-994.

Howell, J. R. and M. Perlmutter, 1964. "Monte Carlo Solution of Thermal Transfer through Radiant Media between Gray Walls", J. Heat Transfer, C 86, pp. 116-122.

Marshak, R. E., 1946. "Note on the Spherical Harmonic Method as Applied to the Milne Problem for a Sphere", Phys. Rev., Vol. 71, pp. 443-446.

Modest, M. F., 1975. "Radiative Equilibrium in a Rectangular Enclosure Bounded by Gray Walls", J. Quantitative Spectroscopy and Radiative Transfer, Vol. 15, No. 6, pp. 445-461.

Perlmutter, M. and J. R. Howell, 1964. "Radiant Transfer through a Gray Gas between Concentric Cylinders Using Monte Carlo", J. Heat Transfer, Vol. 86, No. 2, pp. 169-179.

Ozisik, M. N., 1973. Radiative Transfer, John Wiley and Sons, New York.

Ratzel, A. C., 1981. P-N Differential Approximation for Solution of One- and Two-Dimensional Radiation and Conduction Energy Transfer in Gray Participating Media, Ph.D Dissertation, University of Texas.

Seban, R. A. and T. T. Shimazaki, 1951. "Heat Transfer to a Fluid Flowing Turbulently in a Smooth Pipe with Walls at Constant Temperature", Transactions of the ASME, Journal of Heat Transfer, Vol. 73, pp. 803-809.

Siegel, R. and J. R. Howell, 1980. Thermal Radiation Heat Transfer, 2nd edition, McGraw-Hill Book Company, New York.

Sparrow, E. M. and R. D. Cess, 1978. Radiation Heat Transfer, Augmented edition, McGraw-Hill Book Company, New York.

Trent, D. S. and J. R. Welty, 1974. "Numerical Methods in Heat Transfer", Engineering Experiment Station Bulletin No. 49, Oregon State University, Corvallis, Oregon.

Trent, D. S., L. L. Eyler, and M. J. Budden, 1983. TEMPEST - A Three-Dimensional Time-Dependent Computer Program for Hydrothermal Analysis Volume I: Numerical Methods and Input Instructions, Technical Report PNL-4348, Battelle, Pacific Northwest Laboratory, Richland, Washington.

Usiskin, C. M. and E. M. Sparrow, 1960. "Thermal Radiation between Parallel Plates Separated by an Absorbing-Emitting Nonisothermal Gas", Int. J. Heat Mass Transfer, Vol. 1, pp. 28-36.

Viskanta, R. and R. J. Grosh, 1961. "Heat Transfer in a Thermal Radiation Absorbing and Scattering Medium", Proceedings of the International Heat Transfer Conference, p. 820, Boulder, Colorado.

Viskanta, R. and R. J. Grosh, 1961. "Temperature Distribution in Couette Flow with Radiation", Journal of the American Rocket Society, Vol. 31, pp. 839-840.

Viskanta, R. and R. J. Grosh, 1962. "Heat Transfer by Simultaneous Conduction and Radiation in an Absorbing Medium", J. Heat Transfer, C 84, pp. 63-72.

Viskanta, R., 1963. "Interaction of Heat Transfer by Conduction, and Radiation in a Radiating Fluid", Journal of Heat Transfer, Vol. 85, pp. 318-328.

Viskanta, R., 1964. "Heat Transfer in a Radiating Fluid with Slug Flow in a Parallel-Plate Channel", Applied Scientific Research, Vol. 13, pp. 291-311.

Viskanta, R., 1965. "Heat Transfer by Conduction and Radiation in Absorbing and Scattering Materials", J. Heat Transfer, C 87, pp. 143-150.

Viskanta, R., 1965. "Heat Transfer in Couette Flow of a Radiating Fluid with Viscous Dissipation", Developments in Mechanics, pp. 376-402.

Wylie, R. Jr., 1960. Advanced Engineering Mathematics, 2nd edition, McGraw-Hill Book, New York.

Yuen, W. W. and L. W. Wong, 1980. "Heat Transfer by Conduction and Radiation in a One-Dimensional Absorbing, Emitting and Anisotropically-Scattering Medium", Trans. ASME J. Heat Transfer, Vol. 102, No. 2, pp. 303-307.

APPENDICES

APPENDIX A

P-1 APPROXIMATION COEFFICIENTS A_n^m EXPRESSED IN TERMS OF THE MOMENTS OF INTENSITY

APPENDIX A

P-1 APPROXIMATION COEFFICIENTS A_n^m EXPRESSED IN TERMS OF THE MOMENTS OF INTENSITY

The P-1 approximation of the expansion of the expression for the angular distribution of intensity is given by

$$I(R,\Theta,\phi) = \sum_{n=0}^{1} \sum_{m=-n}^{n} A_n^m(R) Y_n^m(\Theta,\phi) \tag{2.14}$$

where

$$Y_n^m(\Theta,\phi) = \left[\frac{2n+1}{4\pi} \frac{(n-m)!}{(n+m)!}\right]^{1/2} e^{jm\phi} P_n^m(\cos\theta) \tag{2.15}$$

Using the definitions for the associated Lengendre polynominals, P_n^m ($\cos\Theta$) given in Table 2.1 the double series represented by Equation 2.14 may be expanded to yield

$$I(R,\Theta,\phi) = \frac{1}{2\sqrt{\pi}} [A_o^o - \sqrt{3}A_1^o\cos\Theta - \sqrt{3/2}\,\sin\Theta(A_1^1 - A_1^{-1})\cos\phi$$

$$+ j(A_1^1 + A_1^{-1}\sin\phi)] \tag{2.18}$$

The coefficients A_n^m can be expressed in terms of the moments of intensity by substituting Equation 2.18 into Equations 2.19 through 2.22 which define the different moments of intensity, and performing the appropriate integrations. For the P-1 approximation, expressions derived from the first three moment equations are required.

The resulting equations are albegraically solved to yield the following definitions for the A_n^m coefficients

$$A_o^o = 1/2\sqrt{\pi}\ I_o \tag{A.1}$$

$$A_1^o = \sqrt{3}/2\sqrt{\pi}\ I_1 \tag{A.2}$$

$$A_1^{-1} = \sqrt{3}/2\sqrt{\pi}\ (I_2 + jI_3) \tag{A.3}$$

$$A_1^1 = -\sqrt{3}/2\sqrt{2\pi}\ (I_2 - jI_3) \tag{A.4}$$

When these definitions are substituted back into Equation 2.14 the intensity is then expressed in terms of the moments.

$$I(R,\Theta,\phi) = 1/4\pi\ [I_0 + 3I_1\cos\Theta + 3I_2\sin\Theta\cos\phi + 3I_3\sin\Theta\sin\phi] \tag{A.5}$$

APPENDIX B

ANALYTICAL SOLUTIONS FOR THE P-1 APPROXIMATION FORM OF THE RADIANT ENERGY TRANSFER EQUATION

APPENDIX B

ANALYTICAL SOLUTIONS FOR THE P-1 APPROXIMATION FORM OF THE RADIANT ENERGY TRANSFER EQUATION

The radiant energy transfer equation, when simplified using the P-1 spherical harmonics approximation, yields a single second-order partial differential equation of the form

$$1/3\kappa \; \nabla^2 I_o = -a \; [4\pi I_b - I_o] \tag{2.40}$$

where I_b is the black-body intensity and I_o is the zeroth moment of intensity. When this expression is applied to simple one-dimensional geometries and absorption is assumed negligible (i.e., radiative equilibrium), an analytical solution may be obtained for the heat transfer between surfaces.

B.1 PARALLEL PLATE GEOMETRY

The first case considered is the heat transfer between infinite parallel gray plates at different temperatures. If absorption is assumed negligible, Equation 2.40 reduces to

$$\frac{d^2 I_o}{d_x^2} = 0 \tag{B.1}$$

The solution to this expression is

$$I_o = -B - A_x \tag{B.2}$$

where A and B are constants of integration.

The boundary condition at the surface is given by

$$q_w = \frac{\varepsilon_j}{2(2-\varepsilon_j)} [4\pi I_b - I_o] \tag{4.45}$$

To be compatible with Equation B.2, the term q_w, which is identical to I_1 in the x-direction, must be defined in terms of I_o. This is done using the expression

$$q_w = I_1 = \frac{1}{3\kappa} \frac{\partial I_o}{\partial x} \tag{2.36}$$

Therefore, the boundary conditions at surfaces 1 and 2 are

$$@\ x = x_1;\ (dI_o/dx)_1 = \frac{3\kappa\varepsilon_1}{2(2-\varepsilon_1)}\ (I_o - 4\pi I_{b1}) = C_1\ (I_o - 4\pi I_{b1}) \tag{B.3}$$

$$@\ x = x_2;\ (dI_o/dx)_2 = \frac{3\kappa\varepsilon_2}{2(2-\varepsilon_2)}\ (I_o - 4\pi I_{b2}) = C_2\ (I_o - 4\pi I_{b2}) \tag{B.4}$$

where $C_1 = 3\kappa\varepsilon_1/2(2-\varepsilon_1)$ and $C_2 = 3\kappa\varepsilon_2/2(2-\varepsilon_2)$.

Substituting in Equation (B.2), the expressions become

$$@\ x = x_1;\ \ -A = C_1\ (-B - Ax_1 - 4\pi I_{b1}) \tag{B.5}$$

$$@\ x = x_2;\ \ -A = C_2\ (4\pi I_{b2} + B + Ax_2) \tag{B.6}$$

To determine the constants A and B, cast Equations B.5 and B.6 in matrix form.

$$(1 - C_1x_1)A - C_1B = -C_1 4\pi I_{b1} \tag{B.7}$$

$$(1 + C_2x_2)A + C_2B = C_2 4\pi I_{b2} \tag{B.8}$$

Therefore,

$$A = \frac{C_1C_2\ 4\pi\ (I_{b2} - I_{b1})}{[C_2(1 - C_1x_1) + C_1(1 + C_2x_2)]} \tag{B.9}$$

$$B = \frac{4\pi\ [C_2\ I_{b2}\ (1 - C_1x_1) + C_1I_{b1}\ (1 + C_2x_2)]}{[C_2\ (1 - C_1x_1) + C_1\ (1 + C_2x_2)]} \tag{B.10}$$

Substituting Equation B.9 into the definition of I_1 expressed in Equation 2.36, the solution for heat transfer rate between parallel plates is

$$I_1 = \frac{1}{3\kappa} \left(\frac{dI_o}{dx}\right)_1 = - \frac{A}{3\kappa}$$

$$= - \frac{C_1 C_2 \, 4\pi \, (I_{b2} - I_{b1})}{3\kappa \, [C_2(1 - C_1 x_1) + C_1(1 + C_2 x_2)]}$$

$$= - \frac{4\pi}{3\kappa} \frac{(I_{b2} - I_{b1})}{\frac{1}{C_1} + \frac{1}{C_2} + x_2 - x_1} \qquad \text{(B.11)}$$

Back substituting for C_1 and C_2, the expression becomes

$$I_1 = \frac{\pi \, (I_{b1} - I_{b2})}{[1/\varepsilon_1 + 1/\varepsilon_2 - 1 + 3\kappa/4 \, (x_2 - x_1)]} \qquad \text{(B.12)}$$

The Stefan-Boltzmann law states that $\pi I_b = \sigma T^4$ for a given surface. Therefore,

$$I_1 = q = \frac{\sigma \, (T_1^4 - T_2^4)}{[1/\varepsilon_1 + 1/\varepsilon_2 - 1 + 3\kappa/4 \, (x_2 - x_1)]} \qquad \text{(B.13)}$$

For the case of $\kappa = 0$, this reduces to the exact expression for heat transfer rate between parallel plates with no participating medium.

$$q = \frac{\sigma\,(T_1^4 - T_2^4)}{[1/\varepsilon_1 + 1/\varepsilon_2 - 1]} \qquad (B.14)$$

B.2 CONCENTRIC CYLINDER GEOMETRY

The second case considered is the heat tranfser between infinite concentric gray cylinders at different temperatures. If absorption is assumed negligible, Equation 2.40 reduces to

$$1/_r \; d/dr\,(r \; dI_o/dr) = 0 \qquad (B.15)$$

The solution to this expression is

$$I_o = -B - A \, \ell n \, r \qquad (B.16)$$

where A and B are constants of integration.

The boundary conditions at the inner and outer surfaces are

$$@\ r = r_i;\ (dI_o/dr)_i = \frac{3\kappa\varepsilon_i}{2(2-\varepsilon_i)}\ (I_o - 4\pi I_{bi}) = C_i\ (I_o - 4\pi I_{bi})$$

(B.17)

$$@\ r = r_o;\ (dI_i/dr)_i = \frac{3\kappa\varepsilon_o}{2(2-\varepsilon_o)}\ (I_o - 4\pi I_{bo}) = C_o\ (I_o - 4\pi I_{bo})$$

(B.18)

where $C_i = 3\kappa\varepsilon_i/2(2-\varepsilon_i)$ and $C_o = 3\kappa\varepsilon_o/2(2-\varepsilon_o)$.

Using the same method of solution as before, the expressions for A and B are determined to be

$$A = \frac{C_i C_o\ (I_{bo} - I_{bi})}{[C_o\ (1/r_1 - C_i \ln r_i) + C_i(1/r_o + C_o \ln r_o)]} \tag{B.19}$$

$$B = \frac{[C_o\ I_{bo}\ (1/r_i - C_i \ln r_i) + C_i I_{bi}(1/r_o + C_o \ln r_o)]}{[C_o\ (1/r_i - C_i \ln r_i) + C_i\ (1/r_o + C_o \ln r_o)]}$$

Substituting Equation B.19 into Equation 2.36, the solution for heat transfer rate between concentric cylinders is

$$I_1 = 1/3\kappa\ (dI_o/dr)_i = = 1/3\kappa\ A/r_i$$

$$= \frac{4\pi}{3\kappa r_i} \frac{(I_{bi} - I_{bo})}{[\frac{1}{C_i r_i} + \frac{1}{C_o r_o} + \ln\frac{r_o}{r_i}]} \tag{B.21}$$

Back substituting for C_i and C_o and using the Stefan-Bolzmann law, the expression becomes

$$I_1 = q = \frac{\sigma\ (T_i^4 - T_o^4)}{[\frac{1}{\varepsilon_i} - \frac{1}{2} + \frac{r_i}{\varepsilon_o r_o} - \frac{r_i}{2r_o} + \frac{3\kappa}{4}\ r_i \ln\ \frac{r_o}{r_i}]} \tag{B.22}$$

Note that, as $r_i \rightarrow r_o$, the expression approaches the parallel plate solution

$$q = \frac{\sigma\ (T_1^4 - T_2^4)}{[\frac{1}{\varepsilon_i} + \frac{1}{\varepsilon_2} - 1]} \tag{B.14}$$